VALIDATION OF MECHANICAL RESPONSE TISSUE ANALYSIS BY THREE-POINT MECHANICAL BENDING OF ARTIFICIAL HUMAN ULNAS

A Thesis

Presented to

The Honors Tutorial College

Ohio University

In Partial Fulfillment

of the Requirements for Graduation

from the Honors Tutorial College

with the degree of

Bachelor of Science in Biological Sciences

---

by

Patricia A. Arnold

May 2013

This thesis has been approved by

The Honors Tutorial College and the Department of Biological Sciences

_____

Dr. Anne B. Loucks

Professor, Biological Sciences

Thesis Advisor

_____

Dr. Soichi Tanda

Honors Tutorial College, DOS

Thesis Advisor

_____

Jeremy Webster

Dean, Honors Tutorial College

TABLE OF CONTENTS

ACKNOWLEDGEMENTS

This thesis was made possible by funding from the Ohio Space Grant Consortium, the Honors Tutorial College, and the Ohio Musculoskeletal and Neurological Institute. I would like to thank Dr. Soichi Tanda, Dean Jeremy Webster, and Assistant Dean Jan Hodson who have supported me throughout this project and the past four years of college.

I am also grateful for Dr. John Cotton and Will Zaylor of the Department of Mechanical Engineering who contributed to the methodology of the project. I am thankful for the help of Dr. Betty Sindelar of Ohio University's Physical Therapy School for allowing us to use her test frame and laboratory. Amy Johnson of Pacific Research Laboratories/Sawbones® was extremely helpful by agreeing to take this project on and varying the glass fill in the epoxy of the artificial ulnas. I have been lucky enough to have been supported by many members of the MRTA lab during various aspects of this research. I would especially like to thank Nicole Van Horne for her preliminary work on determining how to emulate skin and soft tissue for MRTA testing and Emily Ellerbrock for helping determine the methodology for this project.

Finally, I have been incredibly fortunate to have been advised, guided, and supported throughout this project by the wisdom of Dr. Anne B. Loucks. I would also like to thank Mr. Lyn Bowman for answering every one of my questions and editing every one of my papers during my past three years in the lab. My deepest gratitude goes to Dr. Loucks and Mr. Bowman who have mentored me in all my endeavors as a young researcher.

ABSTRACT

Fracture occurs when mechanical loading exceeds bones strength. The National Institute of Health defines osteoporosis as a skeletal disorder characterized by decreased bone strength, but no medical device measures bone strength directly *in vivo.* Bone stiffness is strongly associated with bone strength, but no clinical method measures bone stiffness *in vivo,* either. Quasistatic Mechanical Testing (QMT) is the reference gold standard method for directly measuring the stiffness and strength of bones, but it can only be employed on excised bones and bone samples.

Mechanical Response Tissue Analysis (MRTA) is a minimal-risk, non-invasive, radiation-free technique for measuring the bending stiffness of certain long bones, such as the ulna, in humans *in vivo*. MRTA was originally developed at Stanford University in the 1980's, but limited information has been published about its accuracy. Ohio University is further developing an MRTA device and the purpose of the research reported in this thesis was to validate the accuracy, precision, and repeatability of this device by comparison to QMT.

The stiffness of standard and custom artificial human ulnas (N = 39) with -10% to +10% excess glass fill in the glass-epoxy composite emulating cortical bone (Pacific Research Laboratories/Sawbones, Vashon, WA) were measured by MRTA and QMT in 3-point antero-posterior bending with proximal support by an articulating vertical Sawbones® humerus and distal support by the anterior distal radio-ulnar articular surface on a steel block. The load was applied at the mid-point of the posterior border.

The precision and repeatability, respectively, of stiffness measurements were calculated without and with dismounting of ulnas from the humerus between repeated measures. Fifteen of the artificial human ulnas were then fractured by QMT under the same support conditions to determine the relationship between bending stiffness and strength.

Results demonstrated that in our hands MRTA and QMT measurements of bending stiffness in artificial human ulnas were virtually identical (MRTA = 1.001*QMT (R^2 = 0.999), and MRTA measurements would be sufficiently precise (1.0 ± 1.0 %), repeatable (3.1 ± 3.1 %), unbiased and interchangeable (± 5%) with QMT for clinical purposes. Additionally, MRTA and QMT measurements of ulna bending stiffness were both strongly associated (R^2 = 0.97) with QMT measurements of ulna bending strength. If ongoing research finds that Ohio University's MRTA device also achieves sufficient measurement performance in cadaveric human arms and ulnas, then MRTA may eventually prove clinically useful for measuring ulna stiffness, estimating ulna strength and predicting fracture risk.

INTRODUCTION

Background on Bone Health

The U.S. Surgeon General has reported that bone health is critically important to the overall health and quality of life for all Americans (8). Bones are living organs; alive with cells and flowing body fluids (9). While continually remodeling structure, bones grow stronger with proper diet and physical activity. Additionally, bones serve as a storehouse for minerals that are vital to the functioning of many other life-sustaining systems in the body (8). A composite material, bone is primarily made up of protein in the form of type I collagen and mineral in the form of hydroxyapatite containing calcium and phosphorous (30) . Bones act as the framework of the body, conferring rigidity and strength to protect vital tissues while still maintaining some degree of elasticity (19, 8). Unhealthy bones have increased fragility that prevents the skeleton from functioning optimally. It is expected that by 2020, half of Americans over the age of fifty will have weak bones and be at risk for fracture (9).

Fractures occur when a mechanical load exceeds bone strength. Bone fractures can occur in a multitude of ways (e.g., compression and torsion) but, within this thesis, the term bone strength will be understood to refer to the force at which a bending bone fractures. Bone strength varies with bone mineral density and bone quality (25). Bone mineral density is expressed as grams of mineral per area or volume (25). Bone quality refers to architecture, turnover, and damage accumulation (e.g., microfractures) (25). Thus, bone fragility is not exclusively determined by low bone mineral density,

but can be the result of failed material or structural adaptations or both (30). Although, measures of bone density are often used as a surrogate to evaluate the strength of bones, only biomechanical testing of bone provides direct information about the strength of bones (33).

Osteoporosis

Osteoporosis is defined as a skeletal disorder characterized by compromised bone strength predisposing an individual to an increased risk of fracture (25) **(Fig. 1)**. There are two main types of osteoporosis—post-menopausal and senile. Post-menopausal osteoporosis predominantly affects trabecular bone. Trabecular bone is found in the ends, i.e., the epiphyses, of long bones and in the vertebral bodies. It is a loosely organized, porous material that aids in metabolic functions (19). Women experience post-menopausal osteoporosis in the first decade following menopause due to an imbalance of ongoing bone resorption and formation processes caused by a decrease in estrogen.

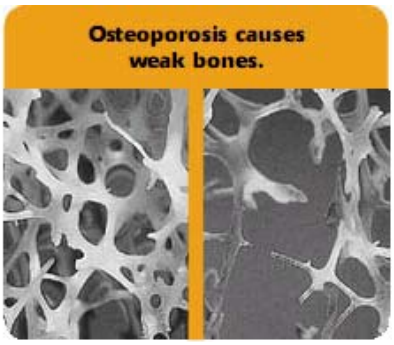

Fig. 1 (above)
Comparison of normal (left) vs. osteoporotic (right) trabecular bone microarchitecture (8)

Senile osteoporosis primarily affects cortical bone. Cortical bone **(Fig. 2)** aids in mechanical and protective functions and is found in the shafts of long bones, i.e., the diaphysis, and the surfaces of all bones. It consists of densely packed collagen fibrils forming concentric lamellae that run in perpendicular planes as in

plywood (19). Senile osteoporosis occurs in elderly men and women experiencing reduced mechanical loading, in the microgravity environment of space flight, and in bed rest scenarios (17, 28, 34). Eighty percent of all fractures in old age occur at skeletal sites that are mainly cortical bone and result from increased intracortical porosity and the thinning of the cortical bone at the inner boundary of the cortex (**Fig. 3)** (37 15, 27). Total age-associated bone loss has been shown to be attributable mainly to cortical bone (72.1%) and less to trabecular bone (32.1%) (37). Thus, decreased bone strength in osteoporosis results can result from the loss of trabecular or cortical bone.

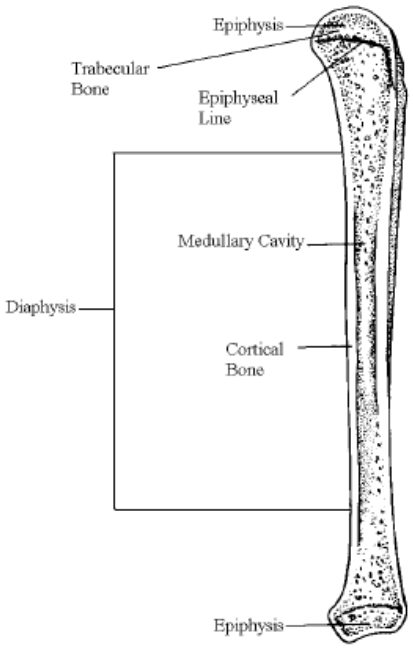

Fig. 2
Diagram of a long bone

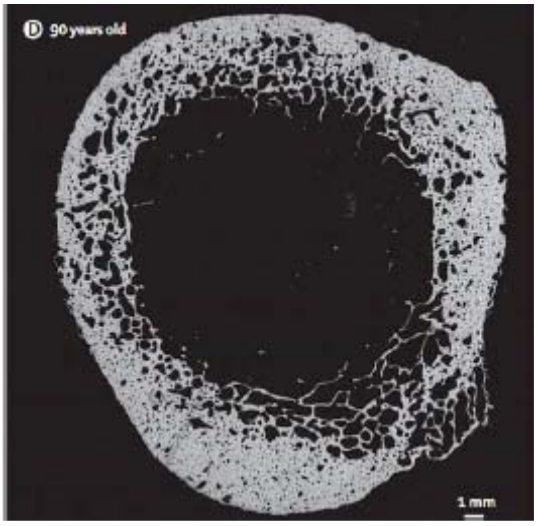

Fig. 3
Micrograph of a 90-year-old woman's femur displaying extreme intracortical porosity. (37)

Dual X-ray Absorptiometry

Currently, there is no *in vivo* clinical method for measuring bone strength (25). Bone mineral density (BMD) values are used as a surrogate measure for diagnosing post-menopausal osteoporosis. Clinically, a technique known as dual x-ray absorptiometry (DXA) is used to measure BMD and diagnose osteoporosis based on T-scores. A T-score is the number of standard deviations an individual is from the mean BMD of a healthy 30-year old of the same sex and ethnicity. Therefore, using DXA measurements, the World Health Organization's (WHO) diagnostic criterion for osteoporosis in post-menopausal women, men over the age of 65, and men between ages 50 and 65 who have other associated risks is a BMD $T \leq -2.5$, that is an individual's BMD is 2.5 standard deviations below the average peak bone density of young adults of the same sex and ethnicity.

Although DXA has been shown to accurately assess bone loss in the trabeculae of post- menopausal women, it poorly captures the cortical bone loss experienced with old age. In a study monitoring the subtrochanteric (below the hip) regions of post-mortem specimens, BMD T-scores correlated poorly with intracortical porosity ($r = –0.28$, $p = 0.19$) (37). About 55% of specimens with BMD T-scores higher than –1.0 standard deviation had high intracortical porosity, while 45% of specimens with BMD T-scores lower than –1.0 standard deviations (indicating clinical bone loss) had low intracortical porosity (37). Inability to detect the bone loss due to increased intracortical porosity causes BMD values to diagnose individuals with osteoporosis who do not sustain subsequent fractures (>96%) and most fractures (81%) to occur in individuals not diagnosed with osteoporosis (31).

DXA is a commonly used tool for diagnosing post-menopausal osteoporosis, but does not reliably estimate bone strength and fracture risk

Other tools assessing bone health for research purposes are peripheral quantitative computed tomography (pQCT) and high-resolution peripheral quantitative computed tomography (HRpQCT). Both of these radiation absorption techniques provide non-invasive measures of the 3-dimensional quantitative and spatial distribution of trabecular and cortical bone in the skeleton. These techniques measure the attenuation of x-rays, which is linearly transformed into hydroxyapatite densities While pQCT and HRpQCT provide insights into bone structure, geometry, and microarchitecture, they, too, like DXA, depend upon epidemiological associations of bone mineral with fractures to estimate bone strength and fracture risk.

Quasistatic Mechanical Testing

Quasistatic mechanical testing (QMT) is the gold standard method for making direct measurements of the strength of materials, including bone, by measuring the forces and displacements required to break a bone. One of the ways QMT measures bone strength is through three-point bending, or flexure, tests. Three-point bending tests are capable of detecting small local variations in elastic modulus (i.e., the material of which the specimen is comprised) but the sensitivity is greatest at midspan, where the bone is cortical, and least at the ends, where the bone

is trabecular (3). When a bone is tested in three-point bending by QMT it is simply supported at each end and a force is applied at midspan **(Fig. 4)** (4). Force is applied from above and the bone bends as compressive forces are applied to the top fibers and tensile forces are exerted on the bottom fibers (4).

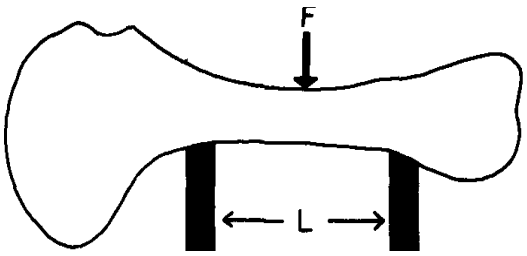

Fig. 4
Three-point testing of a bone in a flexure test. F is the point at which force is applied. L is the length between to the two fulcra points supporting the bone. (4)

Unlike DXA, QMT has found that increasing intracortical porosity directly reduces bone strength. QMT has shown that a 16% increase in intracortical porosity triples the likelihood of bone cracking during deformation (36). While QMT is able to detect changes in bone strength due to increased porosity, the device is limited to excised bones or bone samples. QMT cannot be performed on bones under skin, because some of the measured displacement would be due to compression of the skin instead of bending of the bone. Additionally, bone strength cannot be tested by QMT *in vivo* because QMT measures bone strength by destructively fracturing bone.

In addition to strength, QMT can non-destructively measure bending stiffness (K_b, force divided by displacement) by exerting forces less than the fracture force on the bone and measuring the resulting displacements. Within this thesis, the term K_b should be understood to refer to the force per unit of ulna bending displacement in the antero-posterior direction.

During QMT bending tests, applied force can be plotted against the bending displacement of the bone. In such a load-displacement curve produced during QMT testing of bone, there are two regions: the linear elastic strain region and the non-linear plastic strain region **(Fig. 5)**. These two regions are separated by a yield point, an imaginary boundary that above which the applied force causes permanent damage to the material (33). Permanent damage is referred to as plastic deformation and occurs in the plastic region of the load-displacement curve (33). Bending strength is measured at the end of the plastic region and is the load at which the material fractures (33).

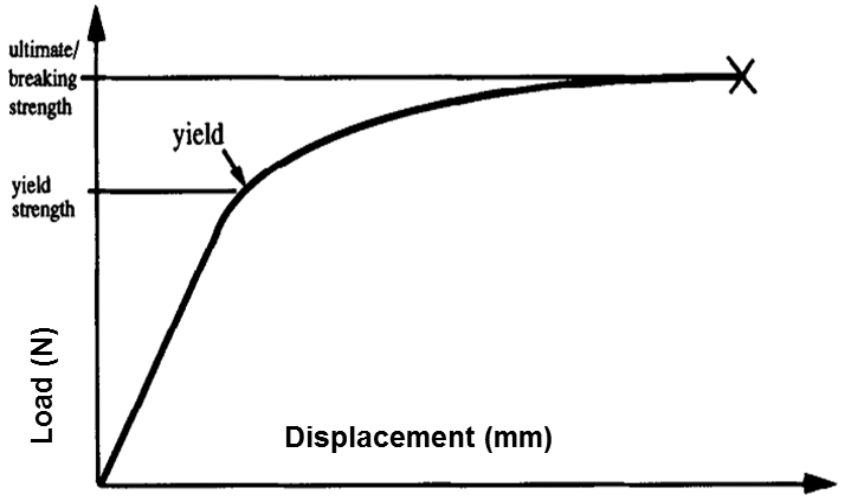

Fig. 5
Force-displacement curve of bone bending during QMT testing. The X at the end of the curve marks the stress and strain at which fracture occurs (33).

K_b is measured as the slope of the elastic region (33). Within in the elastic region, bone behaves as a spring and deformation of the bone increases linearly with increasing load (33). As the load is released, the bone returns to its original shape. QMT measures bone stiffness by applying force only within the elastic region of the curve.

The measure of a specimen's resistance to bending regardless of variations in this test conditions can be calculated from K_b is the called the flexural rigidity (EI) of the specimen (abbreviated $EI = K_bL^3/48$, in units of Nm^2). In EI, E is Young's elastic modulus of the material of which the specimen is comprised, and I is the cross-sectional moment of inertia of the specimen, which quantifies the distribution of that material about the axis of bending (20).

Analogously, in the plastic range of a bending test, a specimen fractures at a load that varies with the distance L between the specimen's supports and with the diameter D of the specimen in the direction of bending. The measure of a specimen's bending strength independent of variations in these test conditions is called the scaled maximum load (abbreviated SML = FxLD, in units of Nm^2, Fx = fracture force.) By accounting for variations in test conditions, EI and SML enable investigators to compare measurements of stiffness and strength that were made under different conditions.

Repeatability, i.e., between trial variability, of K_b measurements by QMT three-point bending has been most often reported in studies examining the stiffness of rat femora. Repeatability for K_b of rat femora has ranged from 7-15% and for

bone strength has ranged from 4-5% (13, 18) However, it is important to note that studies reporting repeatability of stiffness and strength have calculated values based on paired measurements of contralateral limbs, e.g., breaking the left and right rat femur and then calculating the mean, standard deviation and repeatability as the coefficient of variation (standard deviation divided by the mean) of the two measurements. This approach assumes that the right and left limbs of a specimen have equal biomechanical properties and geometry, which may not be so (18).

A strong association has been found between the force at which a bone fractures, the bending strength, and the slope of the elastic region of a force-deflection curve, K_b (14, 2, 29). K_b and bending strength were highly correlated (R^2 = 0.97) when measured in 45 embalmed cadaveric human ulnae (14) (**Fig. 6)**. In a study measuring fifty-six fresh frozen canine radii, ulnae, and tibiae, EI was calculated from K_b and bone strength was measured as fracture moment (M = FxL/4) (2) And again, in the canine bones, bone strength was highly correlated (r = 0.962) with EI (2) (**Fig. 7)**. When EI was measured on the tibias of twelve fresh frozen monkeys, a strong relationship (R^2 = 0.978) was found with bending strength, measured as scaled maximum load (29). Therefore, the K_b and EI are expected to have a strong association with bone strength.

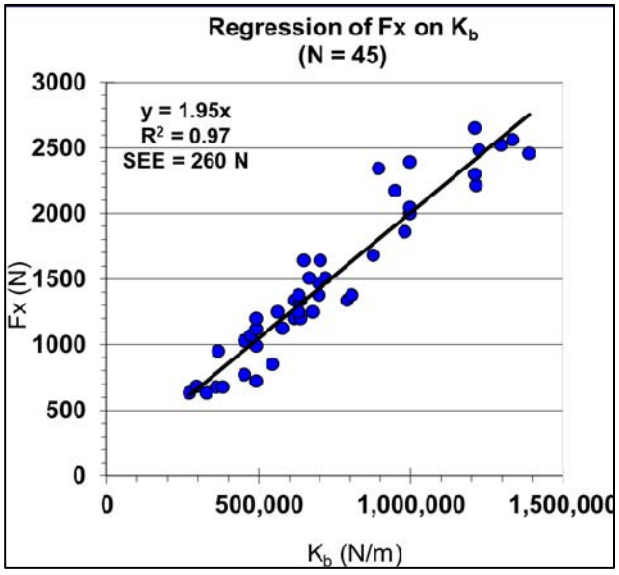

Fig. 6
Relationship between fracture (Fx) and stiffness (Kb) measured in embalmed human cadaveric ulnae. $R^2 = 0.97$ (14).

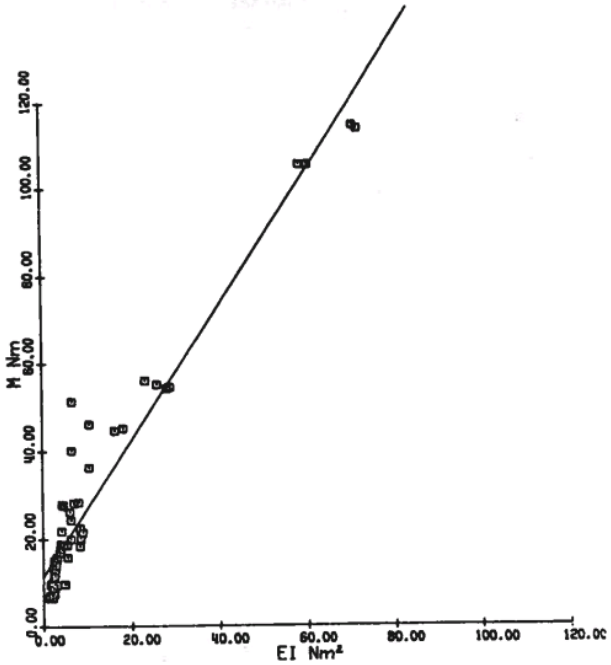

Fig. 7
Relationship between fracture moment (M) and EI measured in canine radii, ulnae, and tibias (r = 0.962). (2).

Although QMT is able to make direct measurements of bending strength and stiffness, it is only applicable to excised bones and cannot be used on humans *in vivo*. Recognizing the need for a clinical device for assessing the fracture risk of bone *in vivo*, Dr. Anne B. Loucks of the Department of Biological Sciences at Ohio University has begun to further the development an alternative approach to fracture

risk assessment known as Mechanical Response Tissue Analysis (MRTA). Collaborating with Dr. John Cotton of the Department of Mechanical Engineering and Mr. Lyn Bowman of the Department of Biological Sciences, Dr. Loucks hopes to develop a device for directly measuring bone health *in vivo* and evaluating senile osteoporosis. This thesis contributes to that effort by attempting to validate MRTA measurements of EI by comparison to measurements made by QMT.

Early Development of Mechanical Response Tissue Analysis

Since current *in vivo* techniques, such as pQCT and DXA, use epidemiological associations to estimate fracture risk from the measurements of bone mineral, they provide only indirect population-based indices of bone strength that are often misleading for individuals (11). QMT directly measures bone strength, but can only be used on excised bones or bone samples. To address these limitations, in 1977 Professor Charles Steele at Stanford University and Dr. Sarah Arnaud at the NASA Ames Research Center began developing a device to monitor the effects of spaceflight on the strength of long bones, such as the ulna and tibia, in monkeys and astronauts *in vivo*. After a decade of effort, a functional Mechanical Response Tissue Analysis system was tested in a clinical setting (20, 24, 23).

MRTA is a non-significant risk, non-invasive, radiation-free technique for making direct functional measurements of the mechanical properties (mass, stiffness, and damping) of long, predominantly cortical, bones in humans *in vivo* (32). In MRTA data collection, bones are oriented in three-point bending while a gentle oscillatory

excitation force (similar to the vibration of an electric razor) spanning a range of frequencies from 40 to 1200Hz is applied by means of a force probe to the skin overlying a long bone, such as the ulna, for a few seconds **(Fig. 8)**. The force and resulting acceleration of the force probe (determined by the mechanical properties of the skin, the underlying bone and nearby soft tissue) are measured and the accelerance ratio (acceleration divided by force) is recorded as a complex (i.e., real and imaginary) function of frequency. **Fig. 9** shows a schematic diagram of the MRTA system.

Fig. 8
MRTA force probe on the forearm

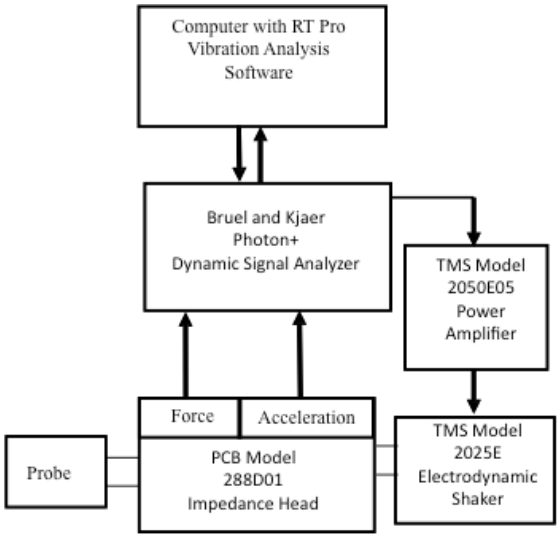

Fig. 9
Schematic diagram of the data collection instrumentation for MRTA

During MRTA data analysis, complex compliance (displacement divided by force) and stiffness (force divided by displacement) frequency response functions (FRFs) are calculated and fitted to a seven parameter mathematical model of the mechanical skin-bone system to estimate the parameters of the model, K_b. As **Fig. 10** shows, the seven-parameter model estimates the mass, stiffness, and damping for both the bone and skin; as well as estimating the parallel damping of the soft tissue. Thus, MRTA is a form of vibration analysis known as parameter estimation. Using the measurement of K_b, MRTA software calculates EI to account for variations in individual ulna length.

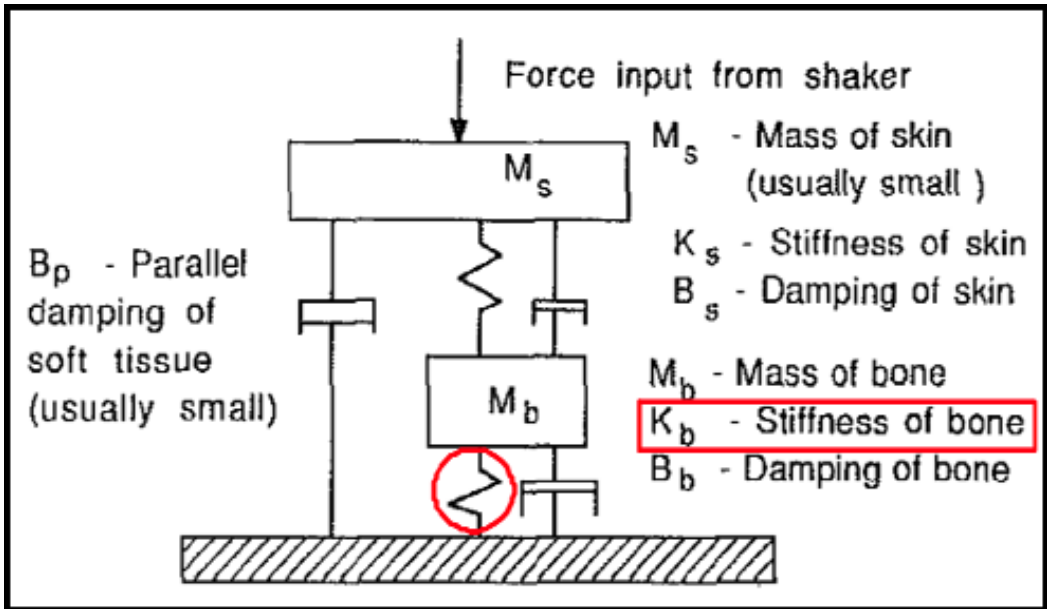

Fig. 10
Seven-parameter mathematical model of the skin-bone system for the forearm (32)

MRTA research thus far has focused on the ulna and the tibia because of their non-invasive accessibility: both bones lie superficially under only thin layers of skin and fat. Compared to the tibia however, the biomechanics of the ulna are much simpler, allowing for a less complicated mathematical model of the skin-bone system and faster data analysis. Therefore, current Ohio University research furthering the development of MRTA technology focuses on the ulna in the hope that measurements of ulna bending stiffness will reflect the strength of cortical bone throughout the skeleton.

MRTA measurements of EI have been previously shown to be strongly associated with fracture risk. When MRTA was used to measure EI on the tibias of twelve fresh frozen monkeys, a strong relationship ($R^2 = 0.915$) was found with scaled maximum load (29). MRTA has also been shown to have strong measurement reproducibility. When four technicians tested four subjects during three different time periods, the precision (within trial variability) of EI measurements with the legacy MRTA devices at Stanford University averaged 4.3% (32). Average repeatability was reported to be 5.3% (32).

In the 1990s, a NASA Small Business Innovation Research-funded effort to commercialize MRTA devices for the diagnosis and treatment of post-menopausal osteoporosis was eventually abandoned, and NASA's investment in the technology was lost. The small business, Gait Scan, Inc., abandoned the technology when the EI of predominantly cortical bone at the mid-shaft of the ulna did not clearly distinguish between post-menopausal women who had been classified as normal, osteopenic, and

osteoporotic. This classification was based on World Health Organization's diagnostic criteria for BMD in skeletal sites comprised of predominantly trabecular bone, i.e., the lumbar spine and proximal femur. It is not surprising that MRTA was unable to distinguish between these types of post-menopausal women since the device measures primarily cortical, rather than trabecular, bone.

After the commercialization effort was abandoned, MRTA systems fabricated by Stanford University and Gait Scan, Inc. were distributed to a few universities for academic research. Since then, clinical trials at Virginia Polytechnic Institute using such legacy MRTA devices have detected large, rapid increases in ulna and tibia EI in response to twenty weeks of resistance exercise training (21, 22). However, such findings could only be reported after discarding 23% of the subject data in ulna tests and 26% of the subject data in tibia tests due to poor quality (22, 21). Other studies with the legacy MRTA devices have reported significant effects of protein degradation on K_b with little change BMD (35).

Further MRTA Development at Ohio University

The previously demonstrated ability of MRTA to detect effects of exercise training on the stiffness of long bones (22, 21) has motivated Dr. Loucks and other Ohio University investigators to initiate a new effort to further develop and commercialize the technology with clinical accuracy and reproducibility. If successfully developed, MRTA would provide clinical insight into the effects of aging, mechanical loading (i.e., exercise) and other interventions on cortical bone

based on direct functional measurements of K_b.

Since the initial commercial development of MRTA was abandoned, a commercial vibration analysis industry has developed for testing the structural integrity of manufactured goods. Ohio University has taken advantage of this industry to improve the vibration technology used in MRTA. The FORTRAN software developed by Stanford University for MRTA data analysis was poorly documented, unsupported, and closed source--leaving users without any access to the source code. As the first organization to examine this source code from Stanford, Ohio University quickly realized that the code was difficult to comprehend and yielded non-unique solutions for values of bone properties. Therefore, Ohio University has created a new method of data analysis written in a more modern and accessible language, MATLAB. This new code identifies optimized estimates of bone properties and reports a measure of quality of how well the data conform to the mathematical model. The measure of quality in Ohio University's software helps researchers to decide whether or not to reject data. The aim of such real-time quality-control of the data is to achieve more accurate estimates of bone properties.

Using these technological advances, Ohio University is the only organization, other than Stanford University and Gait Scan, Inc., to build an MRTA device.

A recently conducted observational study of three trials (consisting of three measurements each) made by three technicians on the ulna bones of six *in vivo* human subjects' gives preliminary estimates of the reproducibility of Ohio

University's MRTA device. The MRTA device has achieved ulna EI measurement precision, repeatability, and technician interchangeability of 1.8%, 3.5%, and 4.3%, respectively (1). These measurements of ulna EI precision (1.8%) and reproducibility (3.5%) are comparable to the precision (4.3%) and repeatability (5.3%) obtained with the legacy devices (32). These values also indicate that Ohio University's MRTA device has preliminarily achieved a clinically acceptable level of measurement reproducibility.

While measurements made by Ohio University's MRTA device have proved to have a strong level of reproducibility, there is no indication of whether or not the values of K_b and EI are accurate. Therefore, the next step in this development program is to validate the accuracy of MRTA measurements of ulna EI and estimates of ulna strength.

Validation of Ohio University's MRTA Device

Accuracy of MRTA measurements can be determined by theoretical or empirical validation. Theoretical validation is performed by measuring EI for a near-ideal uniform beam with MRTA and comparing the measured value to the theoretical value of EI calculated from Young's modulus E for the material and the dimensions of a structure. The dimensions of the beam are used to calculate its moment of inertia I and Young's modulus is taken from the manufacturer's specification for the material from which the beam is made. At Stanford University, one of the legacy devices was validated by comparing EI measurements made on

four round aluminum bars with differing cross-sections to theoretical values (29). Two different mathematical models were used to determine EI of the aluminum rods: the aforementioned seven-parameter model and a six-parameter model. Linear regression analysis demonstrated that MRTA measured EI values determined by both the seven parameter and six-parameter models were strongly associated with theoretical values (R^2=0.998, 0.996, respectively) **(Fig. 11)** (29).

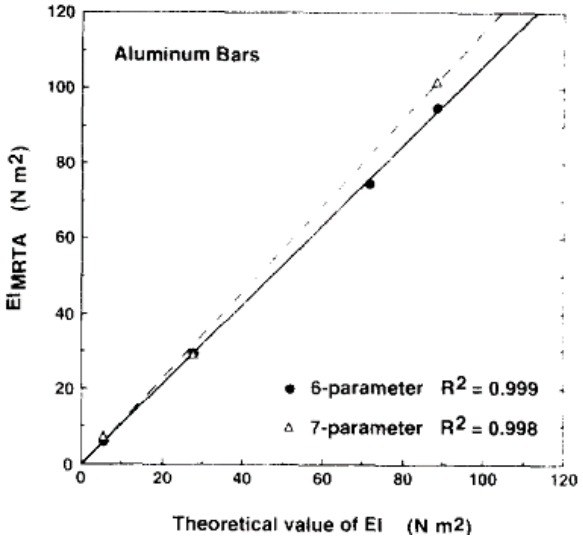

Fig. 11
Theoretical validation of MRTA. EI measured by MRTA in aluminum bars is compared to theoretical value of EI (29)

Empirical validation is achieved by measuring specimen EI by two methods, MRTA and the gold standard reference method, QMT. Stanford University also performed empirical validation with one of the legacy devices (29). EI was measured by MRTA in monkey tibias *in vivo* and then compared to EI measurements by QMT in the postmortem monkey excised tibias (29). When estimated by the six-parameter model EI measured by MRTA was strongly associated (R^2 = 0.947) with EI measured by QMT **(Fig. 12).** EI measured by QMT in the monkey tibias was also strongly related (R^2 = 0.978) to the scaled maximum load (fracture load multiplied by pinned length and anterior posterior diameter) measured by QMT and EI measured by MRTA was also strongly

associated ($R^2 = 0.915$) with scaled maximum load measured by QMT **(Fig. 13)** (29).

Despite strong relationships between EI measurements by MRTA and QMT, the study still reports that EI measured by MRTA was approximately 60% greater than EI measured by QMT (29). This discrepancy was attributed to the use of total limb length in EI calculations by MRTA, and by the length between tibial supports in QMT measurements (29). Actual distance between the points of support in MRTA tests was described as not being precisely known (29).

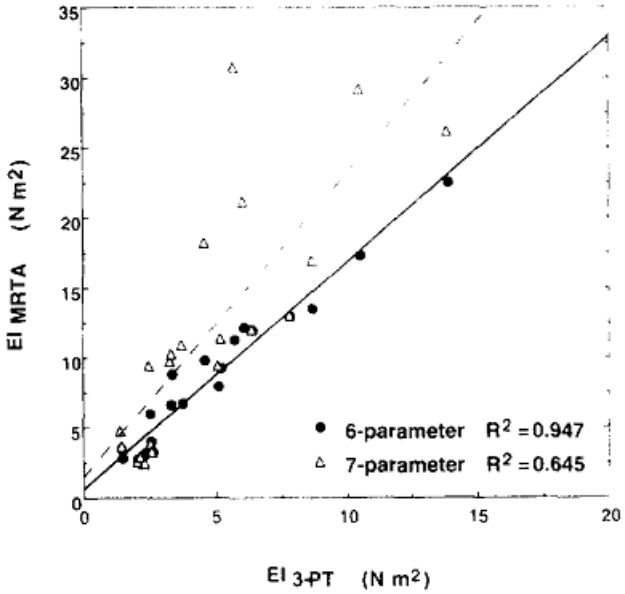

Fig. 12
Linear regression of EI measured by MRTA six-parameter and seven-parameter mathematical models on EI measured by QMT in three-point bending (29)

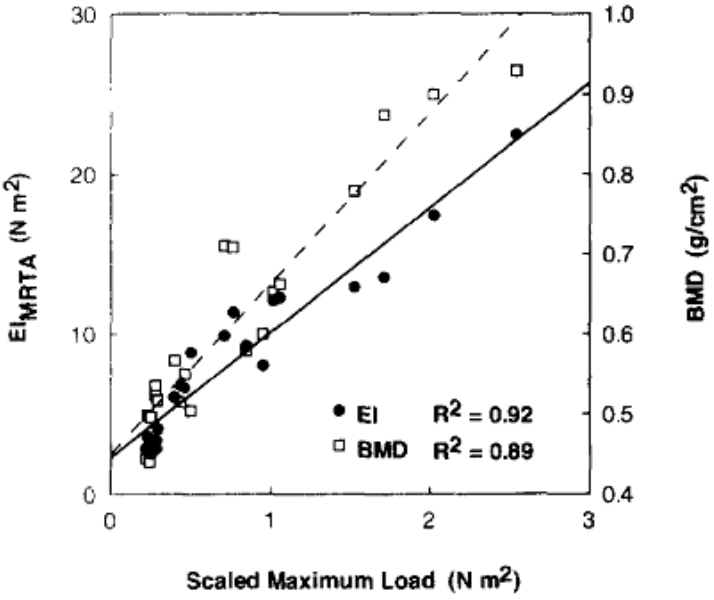

Fig. 13
Linear regression of SML vs. BMD and EI measured by MRTA six-parameter mathematical model by QMT in three-point bending. (29)

While the Stanford study validated MRTA measurements of stiffness, further validation must be done for the Ohio University device. The Stanford study measured monkey tibias, whereas Ohio University measures human ulnas. In the monkey tibias six and seven parameter mathematical models of the skin-bone system were fitted to the data (29), and the seven-parameter model, that OU uses was found to yield a weaker relationship ($R^2 = 0.645$) between tibia EI measured by MRTA and QMT (29). Also, the differences in MRTA and QMT test conditions (i.e., *in vivo* tibias and excised bones) do not allow for a fair assessment of MRTA accuracy.

Bland-Altman analysis of the tibia data measured with the six-parameter model further reveals a large proportional bias between MRTA and QMT methods **(Fig. 14)**. This bias might be attributable to the aforementioned differences between MRTA and QMT testing conditions.

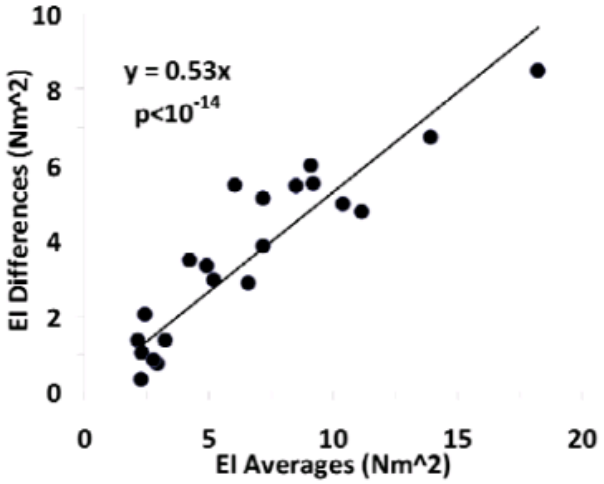

Fig. 14
Regression analysis of the Stanford data reveals a large proportional bias between the two methods.

Elimination of the proportional bias would have still left the random differences shown in **Fig. 15** with limits of agreement (i.e., 95% confidence interval of individual measurements) of ±40%. This level of agreement is too wide to prevent clinical misinterpretations of individual measurements. Thus, legacy MRTA systems were not sufficiently interchangeable with QMT for clinical use.

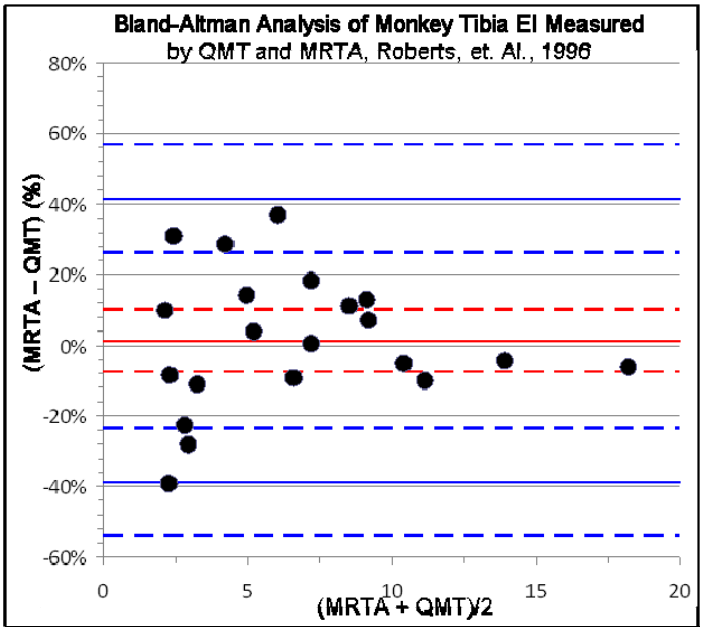

Fig. 15
Bland-Altman analysis reveals random differences after correction for the proportional bias shown above. The dashed and solid red lines indicate the 95% confidence interval of the mean. The dashed and solid blue lines indicate the 95% confidence interval of individual measurements.

While several studies have shown a strong relationship between bone stiffness and strength, no study has compared ulna EI measured by the MRTA seven-parameter model of the skin bone system to bone strength. Furthermore, to the best of the author's knowledge, no study has determined the accuracy of MRTA measurements of bone stiffness by comparison to QMT measurements of stiffness in the same range of force used in MRTA. Therefore, validation of Ohio University's MRTA device is essential to determine whether MRTA is a useful tool for assessing bone health and specifically measuring bone stiffness *in vivo*.

Validation of Ohio University's MRTA device in measurements of stiffness and estimates of bone strength must be done by comparison to the gold standard reference method QMT and, thus, cannot be carried out *in vivo.* The associations between stiffness and strength measured by QMT have only been found with the use of cadaveric bones, which have stringent usage and preservation requirements (10). Human cadaveric bones are costly and difficult to order in large quantities. Artificial human bones with similar mechanical properties to real bones are advantageous to researchers attempting to validate a method because they are readily available, do not degrade over time, and can be controlled for certain variables (e.g., length). Artificial human arm bones (Pacific Research Laboratories/Sawbones®, Vashon, WA) are currently manufactured for orthopedic device testing and are based on geometries of the cadaveric bones from a 90.8kg, 183cm tall male less than 80 years of age (5, 6, 26). These bones are comprised of glass-filled epoxy emulating cortical bone and polyurethane foam emulating trabecular bone. Collaborating with PRL mechanical engineer, Amy Johnson, this project utilized ulnas manufactured with customized amounts of glass fill in the epoxy, allowing for differences in bending stiffness. By varying the amount of glass fill in the epoxy, validation can be carried out with controlled variation in K_b while avoiding uncontrolled variation in geometry and material properties (10). QMT measurements have been shown to have a repeatability of less than 6% when testing artificial human femurs and tibias (12). Sawbones® are of lower cost to the scientific community and studies of the mechanical properties of artificial tibiae,

femurs, and humeri have produced values in the range of human bone (12, 7). Therefore, this thesis employed artificial human ulnas for validation of Ohio University's MRTA device.

Specific Aims

The desired outcome of the research described in this thesis was to validate Ohio University's MRTA device through association with QMT measurements of bending stiffness and bending strength of artificial human ulna bones. Specifically, this project sought to determine:

1. The precision, by calculation of internal coefficients of variation, of:
   1.1 MRTA measurements of flexural rigidity, and
   1.2 QMT measurements of flexural rigidity;
2. The repeatability, by calculation of external coefficients of variation of:
   2.1 MRTA measurements of flexural rigidity, and
   2.2 QMT measurements of flexural rigidity.
3. The association, by linear regression analysis, of MRTA and QMT measurements of flexural rigidity in artificial human ulna bones;
4. The bias and limits of agreement, by Bland-Altman analysis, between MRTA and QMT measurements of flexural rigidity;
5. The association, by linear regression analysis, of ulna bending strength and both MRTA and QMT measurements of flexural rigidity;

The research described in this thesis specifically aimed to:

1. To collect the necessary data including:
    - MRTA and QMT measurements of K_b on artificial human ulnas and then subsequently calculating the EI of each specimen.
    - QMT measurements of bending strength in artificial human ulnas;
2. To perform the necessary statistical data analyses including descriptive statistics, regression analyses, Bland-Altman analyses, and hypothesis tests.

METHODS

Experimental Design

The research described in this thesis attempted to validate Ohio University's MRTA device by determining the accuracy of measurements of ulna EI and associations of EI to ulna bending strength by MRTA relative to measurements of ulna flexural rigidity and bending strength by QMT.

Ulna K_b was non-destructively measured in ulnas by both MRTA and QMT. From ulna K_b, flexural rigidity was determined using the aforementioned Euler solution of a simply supported beam. A portion of the ulnas was then destructively tested to determine bending strength by QMT. **Table 1** below summarizes the experimental design, including the methods of data collection, quantities measured and outcome.

Methods	Dynamic MRTA 3-Point Bending Tests	Quasi-Static Mechanical 3-Point Bending Tests
Measurements	• Oscillatory Force • Oscillatory Acceleration	• Quasi-Static Force • Quasi-Static Displacement • Fracture Force
Outcomes	• Bending Stiffness (K_b) • Flexural Rigidity (EI) • Estimated Bending Strength	• Bending Stiffness (K_b) • Flexural Rigidity (EI) • Measured Bending Strength

Table 1
Experimental design for determining accuracy of MRTA

Hypotheses

The research described in this thesis tested the following null hypotheses:

H_{01}: In linear regression equations of the form y = mx + b used to relate flexural rigidity measured by MRTA and QMT, the y-intercept (b) and slope (m) are both zero.

H_{02}: In Bland-Altman analyses of flexural rigidity measured by MRTA and QMT,

H_{021}: Fixed bias (average difference d) and proportional bias (k in the regression d = kx + c) are both zero.

H_{022}: The 95% confidence interval on differences between paired measurements (i.e., the level of agreement between the two methods) is within an acceptable range of clinical interchangeability, i.e., 10%.

H_{03}: In linear regression equations of the form y = mx + b used to estimate bending strength from flexural rigidity, the y-intercept (b) and slope (m) are both zero.

Test Specimens

To maximize experimental and statistical power for detected relationships between ulna K_b and strength, measurements were made on thirty-nine custom-made Sawbones® artificial human ulna bones **(Fig. 16).** Because of the standard geometry (i.e., length of bone) of the artificial ulnas, calculations of EI to nor K_b to account for individual variations in ulna length were not necessary. Nevertheless, EI was calculated to enable results to be compared to data collected from *in vivo* human ulnas that varied in length.

The Sawbones® ulnas were made with specific, incremental amounts of glass fill above and below the standard percentage of glass fill in the epoxy of bones distributed by Sawbones®. Since the glass filled epoxy emulates cortical bone, the incremental differences in glass fill were expected to create a range of EI values. The ten different percentages of glass fill were: -10%, -7.5%, -5%, -2.5%, 0%, +2.5%, +5%, +6%, +7.5%, +10%, where 0% indicates no change from the standard (i.e., commercially distributed) ulna and the other percentages indicate various increases and decreases in glass fill compared to the standard.

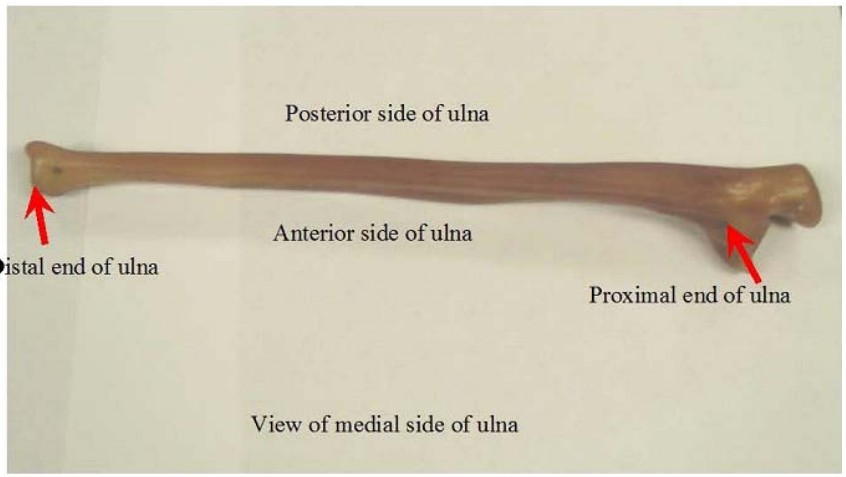

Fig. 16 Sawbones® artificial human ulna.

The MRTA lab ordered the artificial ulnas in four batches, the first two being smaller test batches. Batch 1 consisted of two 0% ulnas, a -7.5% ulna, and a +6% ulna. After having success with MRTA measurements with the first four ulnas, Batch 2 was ordered and included another 0%, -7.5%, and +6% . Wanting to achieve a greater range of EI values in more specific increments, Batch 3 and 4 were ordered. Four ulnas of each level of glass fill were tested except for 0%, which included five ulnas, and 6% which included two. A fifth 0% ulna was ordered because one of the

original 0% ulnas was measured at an abnormally low value of EI. No additional +6% ulnas were ordered after it was decided to order ulnas at increments of 2.5%.

Protocol

Prior to MRTA and QMT testing, all ulnas were weighed and dimensions were measured. Calipers were used to measure the length of each ulna was measured from the point on the distal end to the point on the proximal end that would be directly supported during data collection. The proximal-distal midpoint of the ulna was marked on the posterior side.

All thirty-nine ulnas were non-destructively measured for stiffness by QMT and MRTA. The first seven ulnas were measured first by MRTA and then by QMT. However, the next thirty-two ulnas were measured by QMT first and then MRTA. There was a delay between the testing of the first seven ulnas and testing the rest because of time required for manufacturing. Since the MRTA lab was familiar with using the MRTA device, the first seven were measured with MRTA prior to QMT. After learning how to properly use the QMT test frame, the first seven ulnas were tested with it. QMT data collection proved to be much faster than MRTA and the last thirty-two ulnas were tested on QMT first so that the remaining time could be used to test with MRTA.

During testing of the first seven ulnas, the importance of consistent ulna orientation about its long axis during data collection was recognized as necessary for consistent results. Therefore, the last thirty-two ulnas were marked (explained below) during QMT data collection so that alignment could be quickly repeated for MRTA

data collection. Marking the alignment of the ulnas helped to make QMT and MRTA data collection more efficient.

Fifteen ulnas were then destructively measured by QMT at the end of stiffness data collection. **Fig. 17** illustrates the flow of ulnas through data collection procedures in this project.

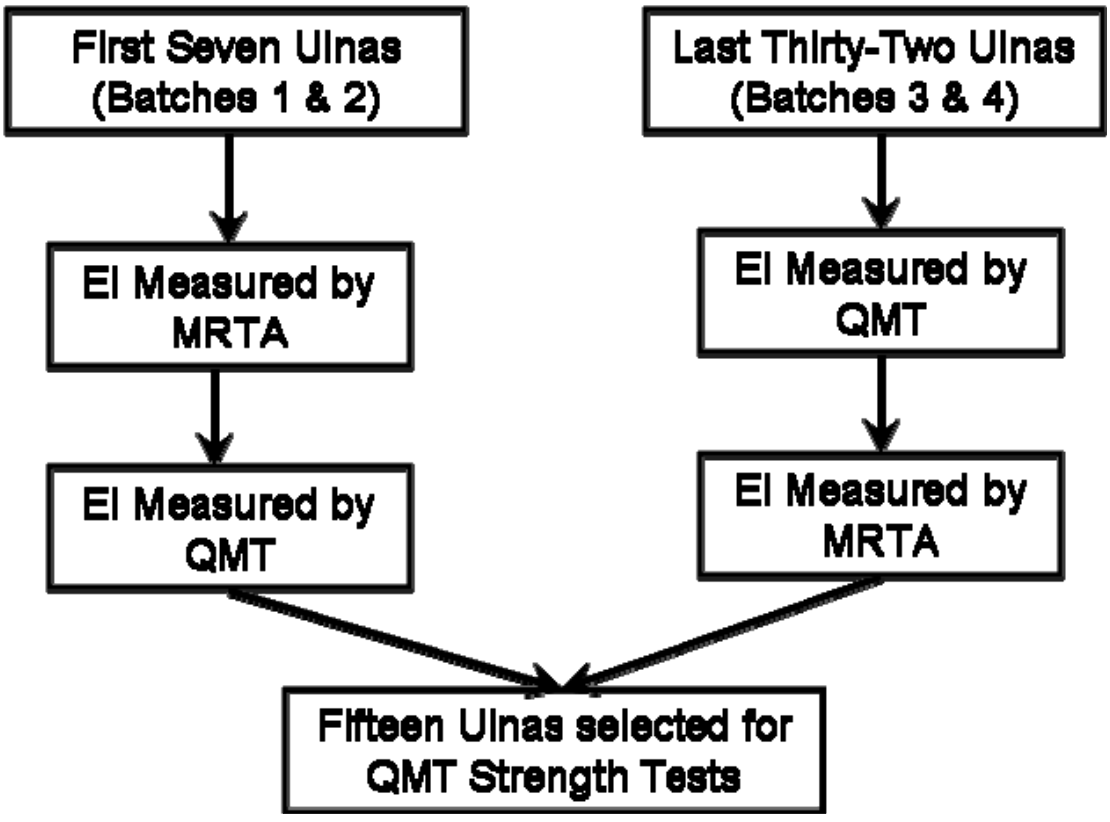

Fig. 17
Protocol used to test artificial ulnas

Data Collection

In both MRTA and QMT bending tests, ulnas were oriented horizontally with their posterior surface up, and the bending load was applied downward on the measured midpoint of the ulna shaft. A vertically oriented artificial Sawbones® humerus supported and articulated with the proximal end of each artificial ulna. Distally, each ulna was supported by the top horizontal flat surface of a vertically oriented 50×75×300 mm steel column parallel to the humerus, as depicted in **Fig. 18** and **Fig. 19**.

Fig. 18
Ulna test setup for QMT data collection

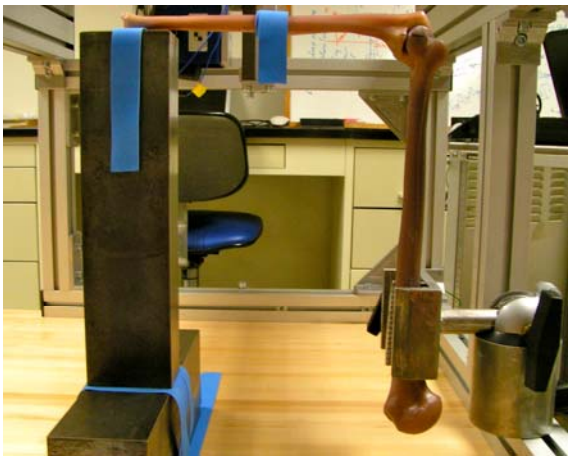

Fig. 19
Ulna test setup for MRTA data collection

The humerus was used for data collection to mimic the *in vivo* elbow joint. The ulna was oriented posterior side up to also mimic *in vivo* testing with MRTA. The ulna was positioned on the humerus during data collection so that when viewing the medial side of the elbow joint, the curvature of the trochlea could be considered a clock face and the tubercle of the coronoid process (**Fig. 20)** of the ulna could be aligned at the 9 o'clock position **(Fig. 21)**. Consistent orientation in this position not only reduced differences between repeated measures of EI by each method, but also reduced differences between MRTA and QMT measurements. Finally, this position of the ulna on the humerus kept the ulna stably in place during data collection.

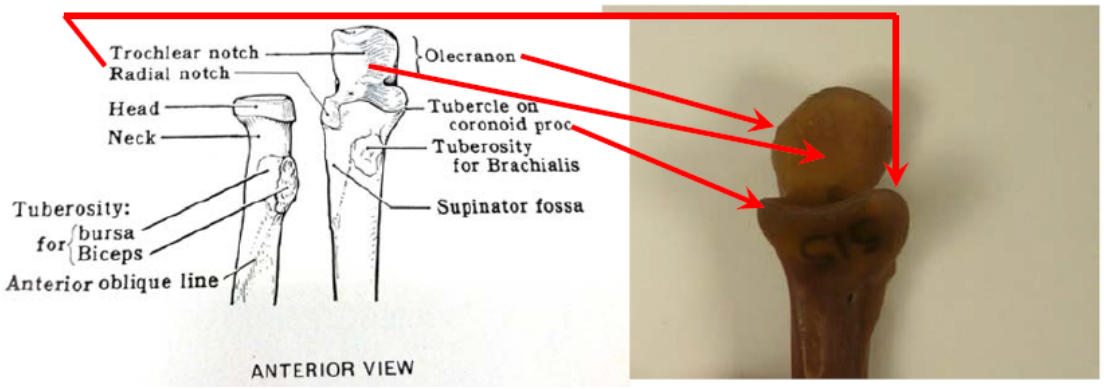

Fig. 20
Bone markers on proximal end of the ulna

The steel blocks were used to support the distal end of the ulna because it was expected that the high level of rigidity in the steel block would allow for stationary support of the distal ulna regardless of the amount of force applied. The same steel blocks were used in MRTA testing and QMT testing.

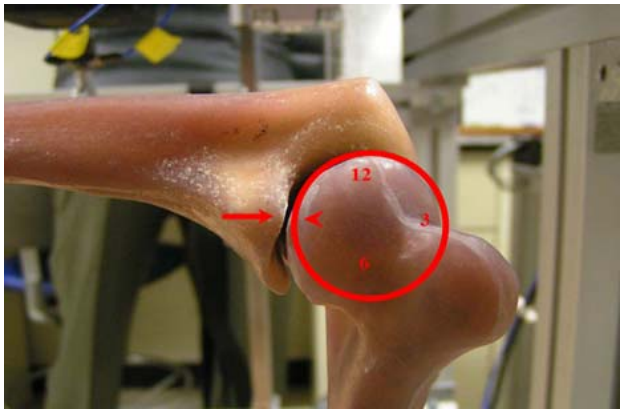

Fig. 21
Alignment of tubercle of the coronoid process with curvature of trochlea

QMT Stiffness Tests

QMT was used to non-destructively measure ulna K_b and destructively measure ulna bending strength. Ulnas were supported in the same orientation for K_b and strength tests.

The QMT device was activated by using a remote control adjacent to the device **(Fig. 22)**. The 10kN load cell remained attached to the crosshead of the test frame during both stiffness and strength testing conditions. Although the 10kN load cell could have been removed during stiffness testing, it was more convenient to leave it in place and attach the

Fig. 22
QMT Remote control used for adjusting the crosshead and turning on the device

25N load cell to the bottom of it.

During bending stiffness tests, the 25N load cell was attached to the 10kN load cell by a tandem piggyback adapter **(Fig. 23)**. The adapter has a threaded screw at either end and the screw with the larger diameter is attached into the bottom of the 10kN load cell. The tandem piggyback adapter was secured onto the bottom of the 10kN load cell by using an Allen wrench to tighten the top nut so that it firmly contacted the bottom of the load cell **(Fig. 24)**. The 10kN load cell has an electrical male D-connector that was disconnected during stiffness testing.

Fig. 23
Tandem Piggyback Adapter

Fig. 24
Attaching tandem piggyback adapter to 10 kN load cell

The 25N load cell has a black shell surrounding silver metal and was oriented in the correct position when the two silver portions were above and below the black casing with the lettering on the load cell right side up. A hole on the top of the 25N load cell allowed for attachment to the bottom narrower threaded screw of the tandem piggyback adapter. The load cell was partially inserted up the adapter and then the second nut of the adapter was turned until it contacted the top of the 25 N load cell.

The bottom nut was secured into place by use of an Allen wrench. This allowed the adapter to attach the bottom of the 10kN load cell to the top of the 25N load cell and to hold the 25N load cell in place for testing **(Fig. 25)**. The 25N load cell also had an electrical male D-connector that remained unplugged and hung loose until stiffness testing began.

Fig. 25 (above)
Attaching 25 N load cell to the tandem piggyback adapter

To accurately test specimens in three-point bending, the force must be narrowly applied at the center of the bone. Therefore, a probe with a knife-edge was attached to the 25N load cell for ulna testing. To connect the probe to the load cell, a second load cell adapter was attached to the bottom of the 25N load cell. The 25N load cell adapter **(Fig. 26)** was attached to the load cell by using an Allen wrench to screw a hex-head screw through the top of the adapter and into the bottom of the load cell. The probe **(Fig. 27)** was then placed into the adapter. The probe had a metal cylinder at one end and a knife edge on the other. The metal cylinder was placed within the 25N load cell adapter and secured with a pin. The knife edge end was exposed outside of the adapter so that the knife edge ran perpendicular to the long side of the 25N load cell **(Fig. 28)**.

Fig. 26
25 N load cell adapter

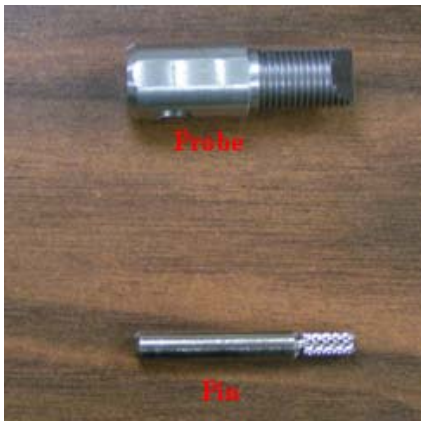

Fig. 27
Probe and pin used in QMT bending stiffness tests

Fig. 28
25 N load cell, adapter, probe, and pin setup

To further secure the probe for testing conditions, a clamp **(Fig. 29)** was pushed up the probe until it contacted the bottom edge of the 25N load cell adapter. The clamp was held in this position by placing a washer directly underneath it and then tightening a nut under it with a wrench **(Fig. 30)**. This kept the probe from moving laterally during data collection. After the probe was secured, the electrical male D-connector was plugged into the female D-connector on the QMT test frame **(Fig. 31)**. Two screws on either side of the adapter locked the D-connector into place.

Fig. 29
Clamp for 25 N load cell

Fig. 30
Load cell setup for QMT bending stiffness tests.

After setting up the 25N load cell for QMT stiffness data collection, the test fixture for the ulna was arranged on the stage of the QMT frame. First, two 50x75x300mm steel blocks were set up on the stage to later support the distal end of the artificial ulna. For the purposes of this thesis, the 75x300mm faces of the steel block will be referred to as the "sides", the 50x300mm faces will be referred to as the "bases", and the 50x75cm faces of the block will be referred to as the "ends" (**Fig. 32).** Please refer to **Fig. 33** for the QMT axis orientation used to describe the rest of the data collection setup.

Fig. 31
D-Connector attachment for 25 N load cell

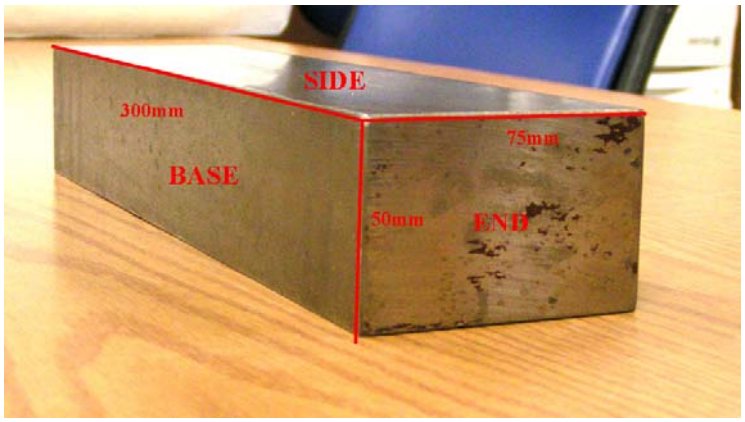

Fig. 32
50x75x300mm steel block with faces defined

The first of the 50x75x300mm blocks of steels was placed onto the left side of the stage, approximately 25.4mm from the left crossbar support **(Fig. 34)**. The steel block was oriented so that the ends of the block were in the Y-plane and the sides of the steel block were in the X-plane. The block was centered on the stage so that equal parts hung over the stage in the X-direction. Markings were made on the stage so that this position could be repeatedly set up in all testing sessions.

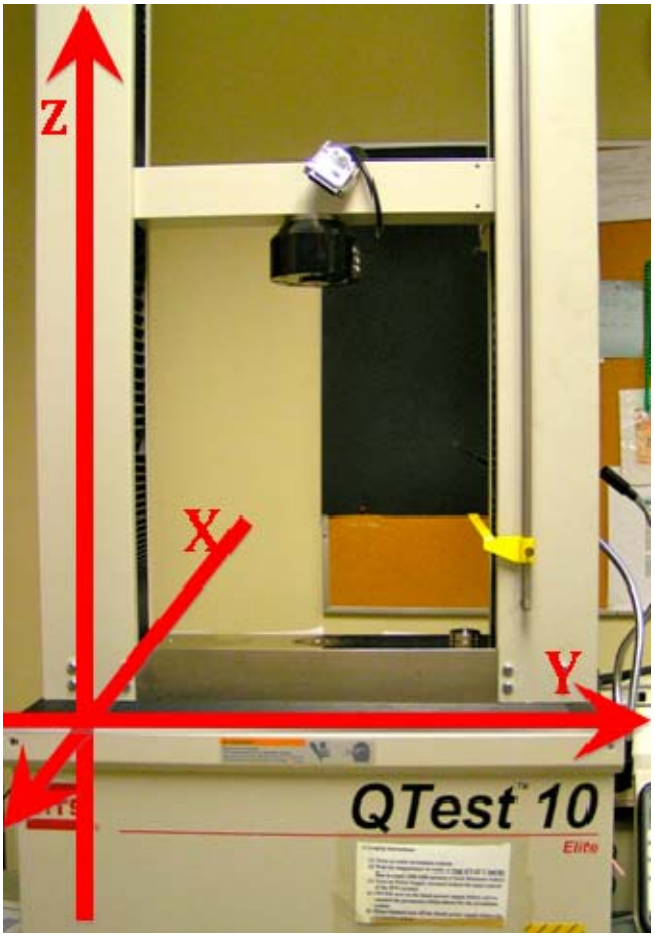

Fig. 33 (above)
Axis orientation of QMT device used to describe data collection setup.

Fig. 34
First steel block laid on the stage of QMT

The second steel block was placed on top of the first so that one end of the second steel block rested upon the exposed side (the one not directly touching the stage) of the first steel block **(Fig. 35)**. The 75mm edge of the second steel block was in the X-plane, the 50mm edge was in the Y-plane, and the 300mm edge was in the Z-plane. The second steel block was placed onto the first so that it was centered with respect to the X and Y-planes. The second steel block was placed on the first steel block 12.5mm inward from both edges of the first steel block in the Y-plane and 112.5mm inward from both ends of the first steel block in the X-plane. Markings were then drawn on the first steel block so that this position could be repeated during different testing sessions.

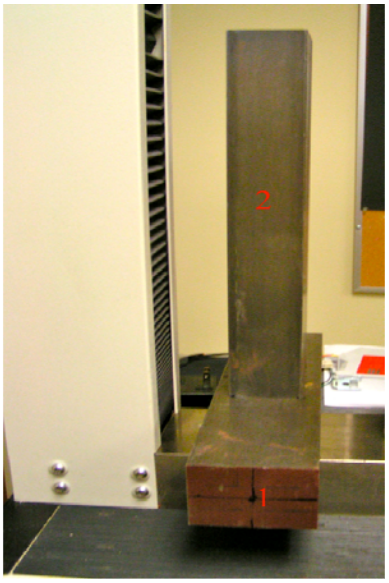

Fig. 35
The two steel blocks used to support the distal end of the ulna setup for QMT data collection.

To prevent the humerus clamp from moving during data collection, a screw secured the humerus clamp through its base and into the QMT test frame. There is a hole in the center of the QMT stage and a slot in the base of the humerus clamp. The slot was aligned over this hole so that the slot was parallel to the Y-axis. A bolt was used to finger tighten the humerus clamp to the stage by screwing it through the slot in the base of the clamp and into the hole in the center of the QMT stage **(Fig. 36)**. The bolt was finger tightened so that adjustments could still be made prior to data collection, but it was tightened with a wrench before testing.

The black swivel handle of the humerus clamp **(Fig. 37)** was used to position the jaws of the clamp directly opposite to the vertical steel block in the Y-direction **(Fig. 38)**. The arm of the clamp was parallel to the Y-axis in this position.

Fig. 36 (above)
A bolt goes through the slot in the base of the humerus clamp and screws into the hole in the stage of the QMT device.

Then, the jaws of the humerus clamp were loosened and separated in the X-direction using the jaws handle. A Sawbones® humerus was placed into the clamp so that the trochlea was upward and positive in the Z-direction and the head of humerus was downward and negative in the Z-direction. On the medial and lateral sides of the humerus are two white mold separation lines that run the length of the humerus from the proximal to the distal end **(Fig. 39)**. Additionally, the inside faces of the jaws of the humerus clamp have notches—three on one side and four on the other. The black jaws handle was used to tighten the jaws around the

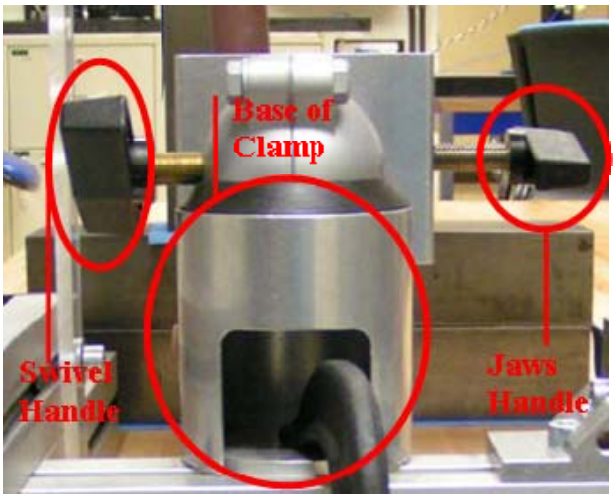

Fig. 37
Parts of humerus clamp

humerus so that the notches on the inside of the jaws articulated with the white mold lines. The white mold line on the medial side of the humerus was positioned so that it fit within the square notch that was most negative in the X-plane of the jaws. On the lateral side of the humerus, the white mold line was positioned so that it fit within the most negative triangular notch in the X-plane of the humerus jaws **(Fig. 40).** The jaws were tightened together so that the humerus clamp firmly gripped and held the humerus in this position. It was necessary to use a 65mm plastic spirit level to ensure that the jaws of the humerus clamp remained level in the Y-plane while they were tightened together. By arranging the humerus in this position the ulna was be able to articulate with the humerus proximally and rest on the steel block distally. This mimics an elbow joint in flexion and resembles how an *in vivo* arm is set up when tested by MRTA.

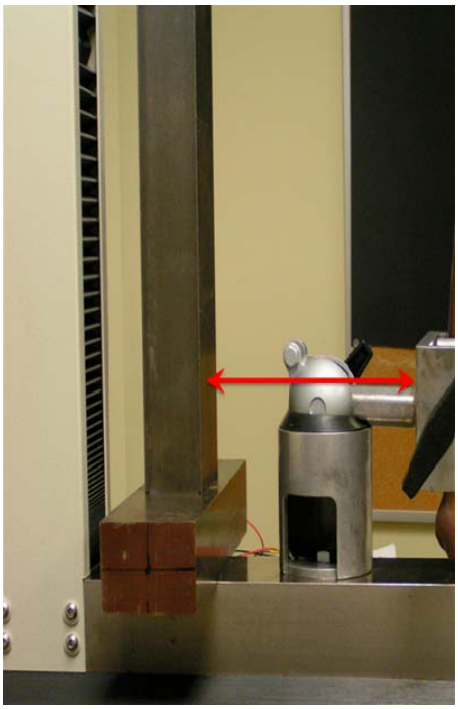

Fig. 38 (above)
Humerus clamp is arranged on stage so that the are directly across from the second steel block.

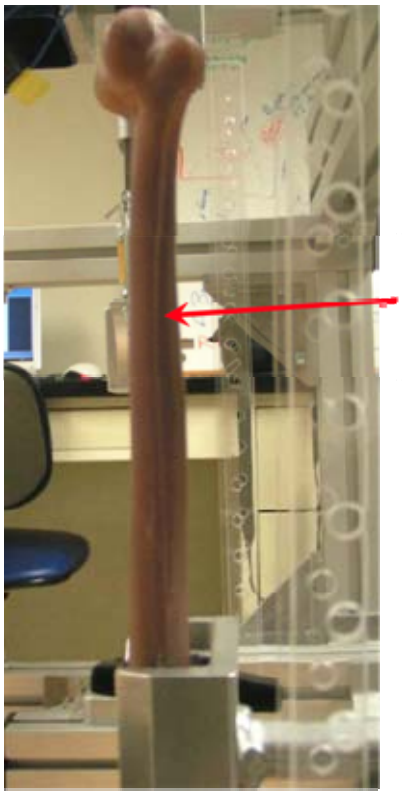

Fig. 39
White mold separation line running down medial side of humerus.

An ulna was placed onto the humerus so that the trochlear notch articulated with the trochlea of the humerus and the distal end rested on the steel block vertical in the Z-plane. The ulna was arranged on the humerus and the steel block so that the posterior border ran parallel to the Y-axis of the QMT device.]

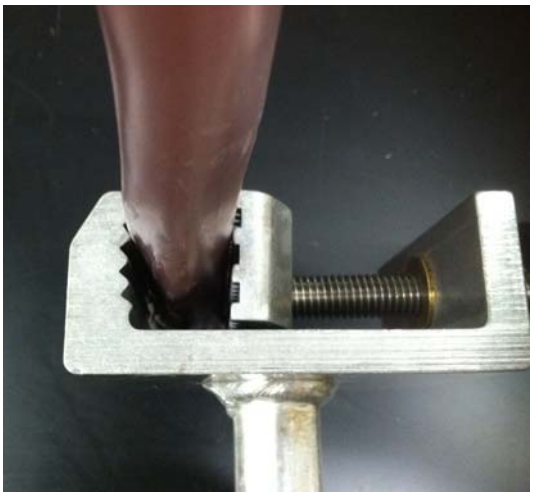

Fig. 40
Humerus fits into the most negative triangular notch in the X-plane and the

Once this orientation of the ulna was established, a plastic spirit level was placed in the Y-direction on the posterior side of the ulna. If the ulna was not level in the Y-direction, the jaws of the humerus clamp were loosened and the humerus was raised or lowered to establish levelness of the ulna. After levelness was established, the humerus was positioned back into the jaws in the previously described orientation and the jaws were tightened again.

The crosshead of the QMT device was lowered so that the probe was 1-2cm above the ulna. The midpoint of the ulna needed to be positioned directly under the probe of the QMT device. There were two ways to move the humerus clamp to align the midpoint of the ulna under the probe. First, the base of the humerus clamp was slid in the Y-direction along the base of the test frame so that the slot in the base was moved around the bolt connecting it to the stage of the device. Secondly, the humerus

clamp was rotated around its vertical axis through the center of the bolt to keep the white mold separation line on the ulna parallel with the X-axis of the test frame as the gap between the curvature of the trochlea and the tubercle of the coronoid process varied by approximately 1-3mm. These two actions were repeated until the midpoint of the ulna was directly beneath the probe of the QMT device. After this position was established, the bolt between the base of the humerus clamp and the stage of the QMT test frame was carefully tightened with a wrench so that the base of the humerus clamp was no longer able to move. The steel block supporting the distal end of the ulna was then marked at the point the distal end of the ulna contacted the block so that each ulna would be aligned in the same positions in the X and Y planes during data collection.

Once the ulna was aligned, the coarse adjustment on the remote control of the test frame was used to lower the probe of the QMT device within 0.5-1cm of the posterior side of the ulna. The fine adjustment was then used to further lower the probe so that light was barely visible between the ulna and the probe without the probe contacting the ulna. The accompanying computer program, Testworks (MTS Systems Corporation, Eden Prairie, MN) was used to display the force input of the load cell and the displacement of the crosshead. Testworks creates a graph of these two measurements as the bone is loaded with up to 25N of force. The stiffness of the ulna is measured as the slope of a force/displacement curve as the load increases.

As the crosshead began to lower and force was applied to the ulna, the elbow joint was observed to ensure that the ulna was stable on the humerus and did not move during data collection. If the ulna did move during collection, the crosshead was

raised and the ulna was rotated around its long axis to increase stability. Stability of the ulna was determined by pinching the diameter of the ulna between the thumb and forefinger in the area between the midpoint of the ulna and the proximal end. Then, the thumb and forefinger were gently moved in the X-direction to detect whether or not the ulna could wiggle within the articulation with the humerus. After assuring stability, the crosshead was lowered in the manner described above and data collection was reinitiated.

Repeated measurements of stiffness were collected until the internal coefficient of variation (standard deviation/mean) was less than or equal to 1.0% for the last five measurements taken consecutively, because QMT measurements would start out at one value and asymptotically increase to a higher value, eventually reaching equilibrium (**Fig. 41)**. After saving the trial (the last five measurements), the crosshead was raised and another ulna was placed onto the humerus into the orientation described above.

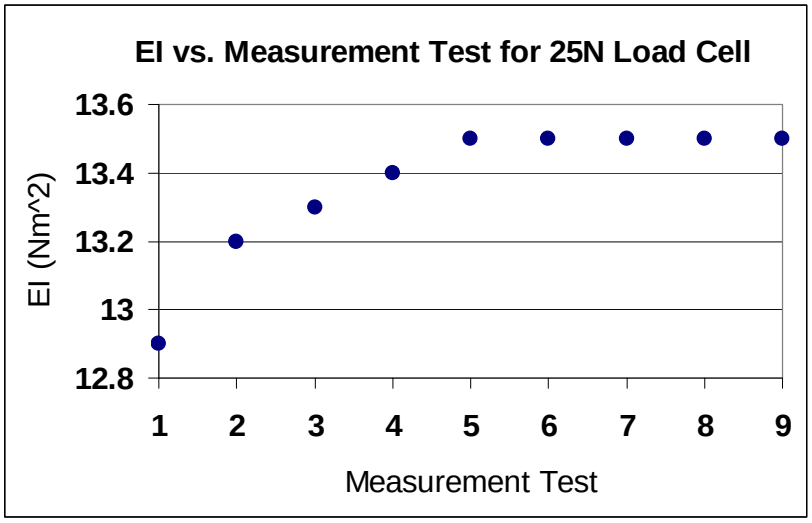

Fig. 41
EI increased asymptotically for the first few tests on each ulna. Consecutive measurements were made until the coefficient of variation (CV) of the last five tests was less than or equal to 1.0%.

QMT Strength Tests

Fifteen ulnas were fractured by QMT to measure bending strength. Ulnas were selected over a range of EI to try to produce a range of bending strength. For measurements of bending strength, the procedure outlined above was repeated for an initial stiffness test. The initial stiffness test was done to ensure that the ulna being tested was oriented in the same way it had been oriented during previous measures of bending stiffness.

After matching the ulna orientation, the crosshead was raised off the ulna and the 25N fixtures were removed from the 10kN load cell. The piggyback adapter was removed from the 10kN load cell. Then, a 10kN load cell adapter was placed into the bottom of the 10kN load cell (**Fig. 42)**. The aforementioned mentioned probe was placed into the load cell and secured with a pin, a clamp, and a nut as it had been previously during stiffness testing (**Fig. 43)**. While setting up the 10kN load cell for data collection, the ulna remained in the same position as it had during the stiffness test.

Fig. 42 (above)
10kN load cell with 10kN load cell adapter attached.

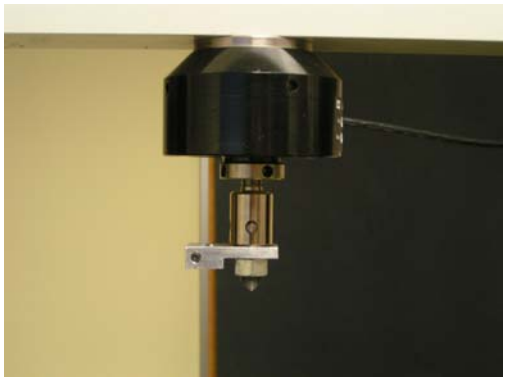

Fig. 43
10kN load cell with 10kN load cell adapter and probe attached.

The crosshead was lowered within 1mm of the posterior side of the ulna and data collection was initiated. Previous research had shown that stiffness measurements made by the 10kN load cell showed the same asymptotic pattern during the first few measurements that the 25N load cell had displayed. To ensure that strength was not measured until the asymptotic limit had been reached, repeated stiffness measurements were made with a peak force of 50N prior to fracturing. Tests were made until the last five consecutive measurements had a CV of 1.0% or less.

After the 50N tests, the fracture test was initialized **(Fig. 44)**. Bones typically fractured within ten minutes.

Fig. 44
Ulna bending during bending strength test.

For the final three ulnas measured for bending strength, a different setup was employed. Previous data collection, recorded with a video camera, had shown that the steel block and humerus were shifting when the ulna was subjected to large forces (e.g., 100-500N) during fracture testing. To decrease movement during data collection, the bottom third of the humerus was cut off. This allowed the clamp to grip a larger portion of the total humerus and prevent bending of the humerus during data collection. To reduce friction of the ulna in the trochlea during data collection, a generous amount of petroleum jelly was spread between the

articulation of the ulna and humerus. In addition, petroleum jelly was also spread between the distal end of the ulna and the steel block at the point of contact **(Fig. 45).**

For all tests, force and displacement data were recorded at 10 Hz as the crosshead of the test frame advanced at a speed of 1.608 mm/s. The initial stiffness test EI, the average EI of the last five consecutive 50N tests, the maximum displacement, and the peak force of fracture (i.e., ulna strength) were recorded for data analysis.

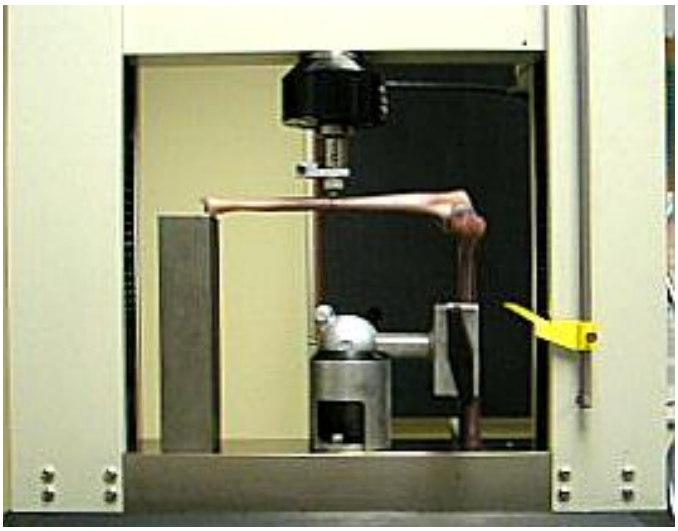

Fig. 45
Strength test with shortened humerus. Petroleum jelly is spread at distal end articulation of the ulna and steel block and proximal articulation of the ulna with the humerus.

MRTA

Ulnas were positioned for MRTA stiffness measurements in position similar to QMT orientation for stiffness measurements. Prior to data collection, the MRTA device was set up for collection data from the artificial ulnas. Refer to **Fig. 46** for axis orientation for axis alignment of the MRTA device. Lying in the Y direction on the head edge of the MRTA table was an orthogonal aluminum beam of the support structure. The base of the humerus clamp was placed on this beam so that the 'jaws' were over the table. The base was not perfectly centered on the aluminum beam; allowing for about 3.8cm of the base to protrude in the X- direction above the table, with no part of the metal beam beneath. The orthogonal beam at the head of the table was attached to three other beams that were vertical in the Z-plane. The humerus clamp was placed a standard 31.8cm inward and towards the center of the table from the most positive vertical beam on the Y-axis. The base of the humerus clamp is a cylinder with a large open section cut out of the back. One end of a large C-clamp was placed within the cut out of the base while the other half wrapped around the bottom of the MRTA table (**Fig. 47**). The C-

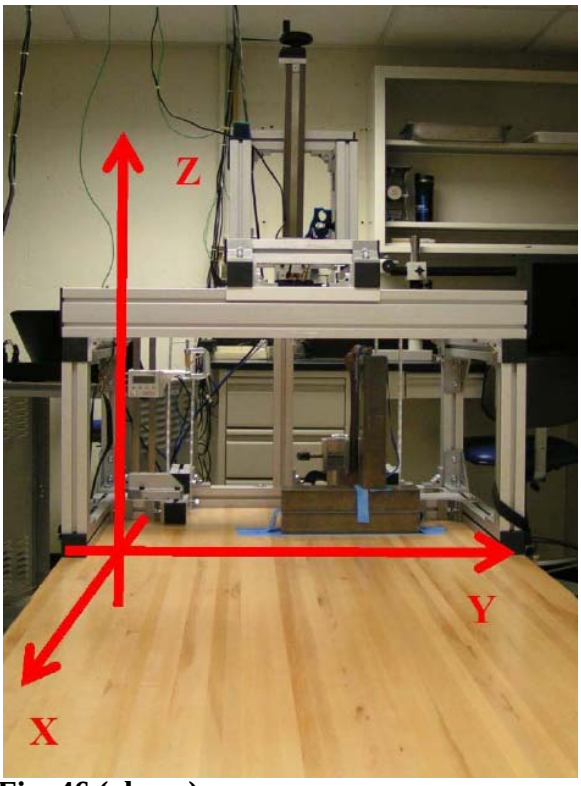

Fig. 46 (above)
Axis orientation for MRTA device.

clamp was tightened to secure the humerus clamp into place.

The swivel handle of the humerus clamp was used to rotate the arm of the clamp so that it was over the table. The arm was aligned so that it ran parallel in the X-direction to the wood grain of the table. The swivel handle was tightened in to place and the levelness of the jaws in the Y-direction was checked**.**

Fig. 47
A C-clamp is used to secure the humerus clamp to the MRTA table.

The jaws handle was used to open the jaws and the humerus was placed into the jaws in an orientation similar to the QMT testing setup. However, the second square notch from the head end of the table on the medial face of the jaws articulated with the white mold separation line on the medial side of the humerus this time. On the lateral side, the white mold separation line fit into the second triangular notch **(Fig. 48)**

Fig. 48
Notches on inside of jaws articulating with humerus

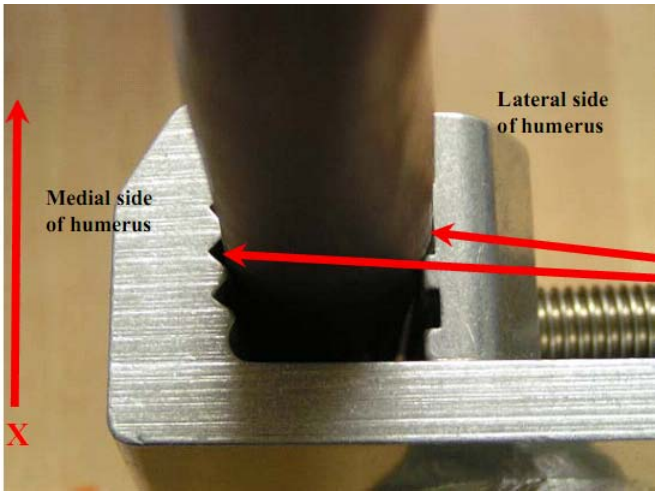

Blue rubber tourniquets (x-tourn™ Cat 18679, Avcor Health Care Products, Ft Worth, TX) were used to prevent vibrations of the mechanical structure from being coupled into the ulna. One was placed 30.5cm away from the orthogonal beam at the head of the table so that it ran parallel to the beam in the Y-direction **(Fig. 49)**. The tourniquet was placed so that in the X-direction it was directly across from the humerus. Three more tourniquets were placed directly next to the first one and in the same orientation **(Fig. 50)**.

Next, a 50x75x300mm block of steel was placed onto the four tourniquet straps **(Fig. 51)**. The steel block was oriented with one of its sides lying on the blue rubber and the other side facing upward in the Z-direction. The 50mm edges of the block were vertical in the Z-plane and the 75mm edges were horizontal in the X-plane. In the X-plane, the block did not completely cover the blue rubber and approximately 1.3cm of blue rubber on the portion closest to the head of the table while 1.1cm was visible on the portion more positive in the X-direction. In the Y-plane, the block was aligned so that it was across from the humerus.

Three more tourniquet straps were then placed on top of the first steel block. These pieces of rubber were positioned in the same orientation as the ones beneath the block. The tourniquet straps lay side by side but did not overlap on top of the block. Then, a second steel block was placed on top of the first and in the same orientation as the first **(Fig.52)**. The edges of the second steel block were made flush with the first.

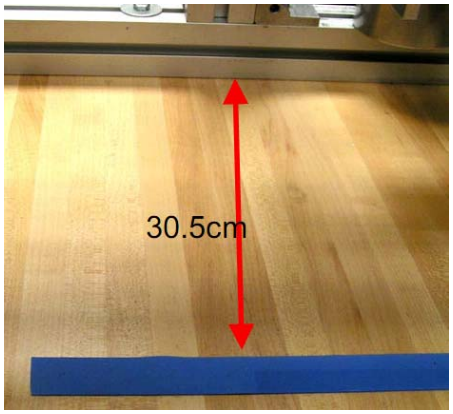

Fig. 49 (above)
Blue rubber tourniquet strap is placed 30.5cm away from orthogonal beam at the head of the table

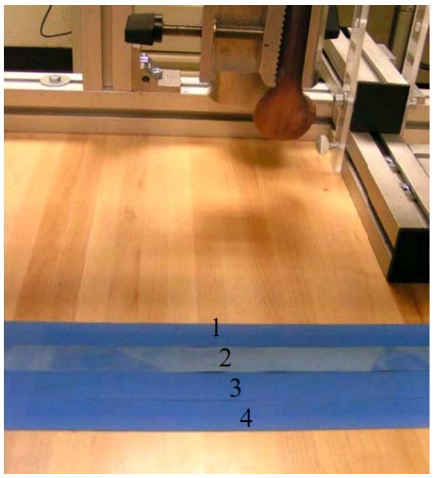

Fig. 50 (above)
Four tourniquet straps lying side by side

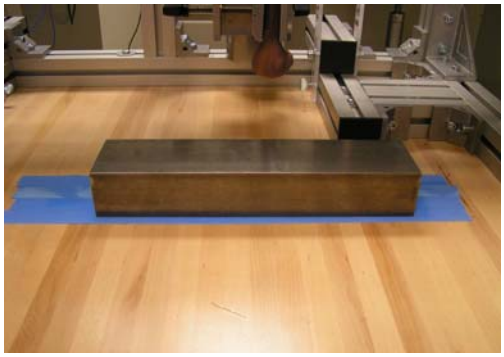

Fig. 51
Steel block is placed on top of four blue rubber tourniquet straps

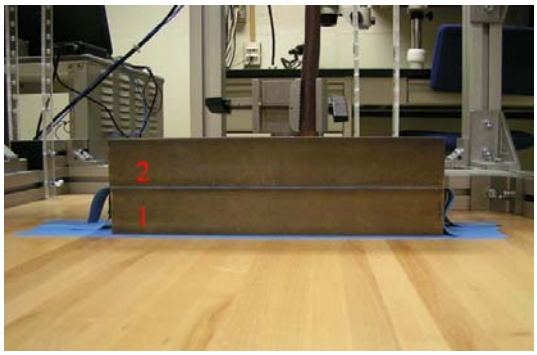

Fig. 52
Second steel block is placed on top of first with three strips of blue rubber in between.

Three smaller pieces of tourniquet strap were laid on top of the second steel block so that they ran lengthwise in the X-direction **(Fig. 53)**. The three straps lay side by side without overlapping and were positioned approximately 9.5cm inward in the Y-direction so that they lined up directly across from the humerus. A third steel block

was positioned so that one of its ends contacted the three pieces of tourniquet strap and other one faced upward in the Z-direction. The 300mm edge of the third steel block was vertical in the Z-direction and the 50mm was horizontal in the Y-direction. The steel block was oriented so that it was parallel to and directly across from the humerus, as with QMT setup **(Fig. 54)**

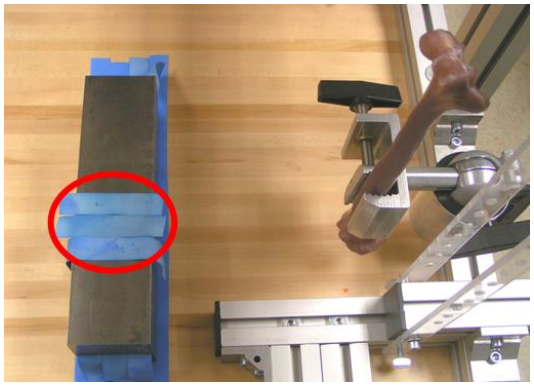

Fig. 53
Three pieces of blue rubber are placed across from the humerus on top of the second steel block.

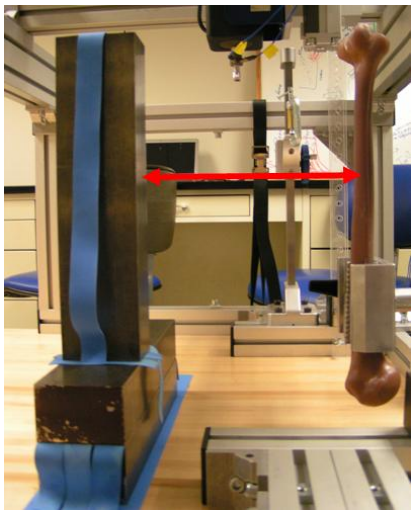

Fig. 54
The third steel block is setup directly across from the humerus.

The proximal end of the ulna was positioned on the humerus as it had been during QMT testing. Markings made on the tubercle of the coronoid process during QMT measurements were used for alignment.

The distal end of the ulna rested on the third steel block. A piece of blue rubber tourniquet strap was placed between the distal end of the ulna and the steel block at the point of contact. The posterior border of the ulna was first set parallel to the X-axis. After levelness had been achieved and checked with a 65mm plastic

spirit level, the midpoint of the ulna was covered with seven wraps of a blue rubber tourniquet strap (**Fig. 55)**. The strap was wrapped tightly with the layers neatly on top of each other. The ulna was placed back onto the proximal end of the humerus in the previous position. However, to increase stability of the ulna during data collection, the distal end of the ulna was placed off center by moving it 1cm laterally. This caused the posterior border of the ulna to no longer be parallel to the X-axis.

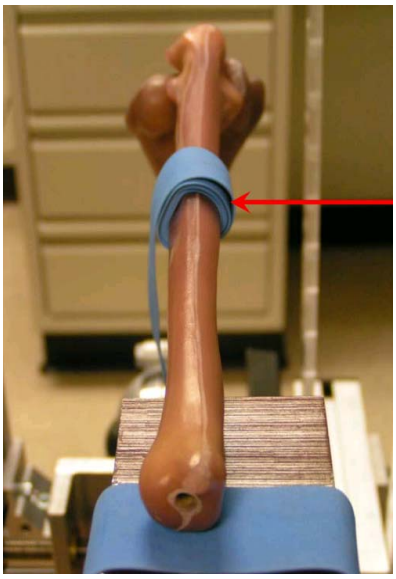

Fig. 55
Seven wraps of blue rubber cover the ulna for data collection and distal end rests on a strap of rubber

Stability of the ulna was evaluated by pinching the proximal half of the ulna with the thumb and forefinger and gently shaking it back forth in the Y-direction. The ulna was considered stabilized when no wiggling was felt between the proximal end of the ulna and the humerus. It was necessary to evaluate the stability of the ulna to prevent vibrations from occurring between the ulna and the humerus at the elbow joint. The upper stage of the MRTA device was adjusted along the X and Y axes to align the force probe on the bottom of the linear module over the midpoint of the ulna and the blue rubber. The force probe was centered on the blue rubber along the X-axis and was intentionally misaligned slightly medial to the posterior border of the ulna along the Y-axis with one third of the probe not contacting the ulna **(Fig. 56)**. The probe was lowered until it contacted the blue wraps of rubber.

In this project, a static preload force of approximately 21 N was applied via the mechanical force probe to the wraps of rubber emulating soft tissue covering the underlying artificial ulna. Then, an electromechanical linear motor (Model K2007E01, The Modal Shop, Cincinnati, OH) was used to superimpose on the static force an oscillating force with amplitude of approximately1N spanning a range of frequencies from 40 to 1200 Hz. The applied force and resulting acceleration of the force probe determined by the mechanical properties of the mechanical skin-bone system was measured with an impedance head (Model 288D01, PCB Electronics, Depew, NY) mounted in line with the force probe, and converted to a complex accelerance (acceleration/force) frequency response function (FRF) by means of a dynamic signal analyzer (Photon+, Bruel & Kjaer, Naerum, Denmark) **(Fig. 9)**. These FRFs were displayed and processed by the computer program RT Pro (Bruel & Kjaer, Naerum, Denmark) during data collection. From accelerance, a complex compliance (displacement/force) FRF was derived and also displayed during data collection **(Fig. 57).**

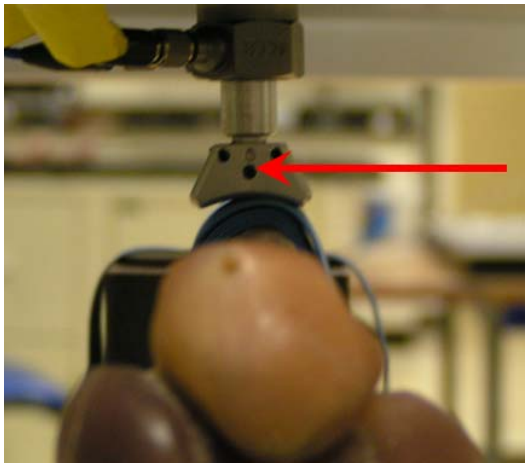

Fig. 56
Probe was set off center in Y-direction ulna.

Data analysis was used to fit the 7-parameter model of the skin bone system to the raw data collected with MRTA. Thus, best results were achieved when the accelerance and compliance waveforms displayed during data collection closely resembled the seven-parameter model. Within the seven-parameter model, compliance and accelerance both have two distinct resonance peaks, a low frequency peak primarily determined by the mass stiffness and damping of the bone and a high frequency peak primarily determined by the mass stiffness and damping of the skin **(Fig. 57)**. The setup described previously was consistently able to collect raw data off of the artificial ulnas with distinct "bone" and "skin" peaks. Raw data needed to be

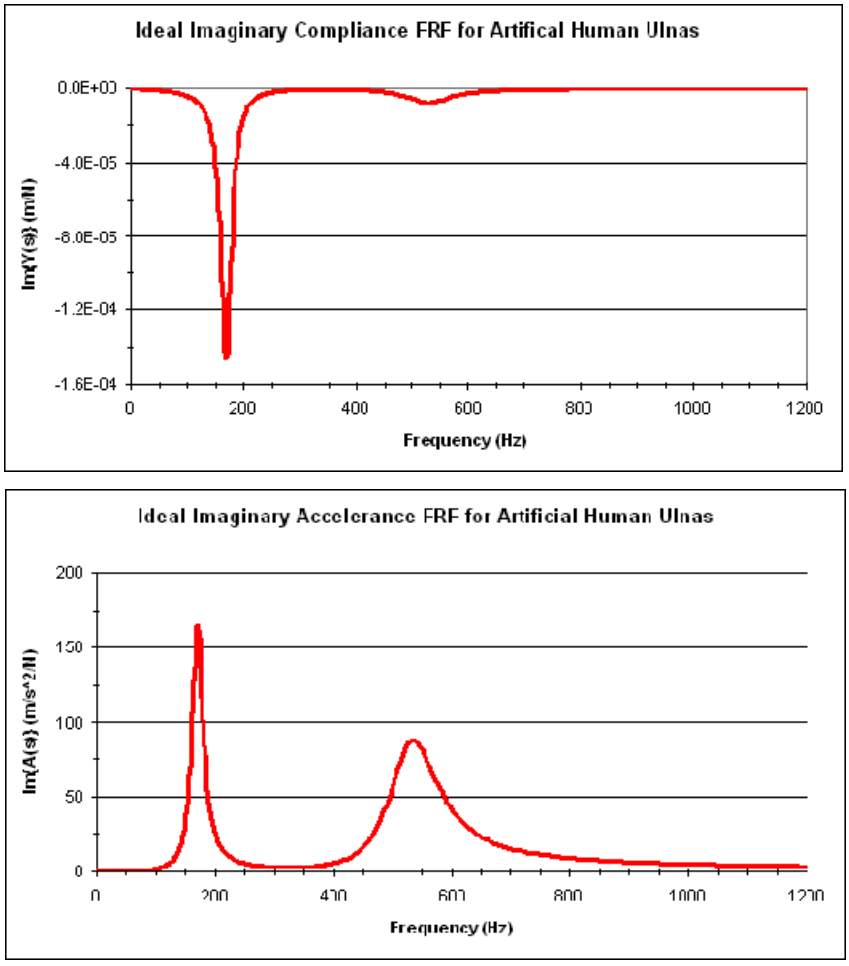

Fig. 57
Ideal imaginary compliance (top) and accelerance (bottom) FRFs.

thoroughly examined to ensure that the occurrence of additional non-ideal peaks was minimal. Frequently, non-ideal peaks occurred in the frequency region to the left of the bone peak and were more obvious in the compliance graph than the accelerance graph. For that reason, the accelerance graph in RT Pro was set to display the entire range of frequencies, 40 to 1200Hz **(Fig. 58)**, but the compliance graph was narrowed in on the region before the bone peak, 40 to 220 Hz **(Fig. 59)**. In addition, data was best viewed when the accelerance graph had a Y-axis set from around 0 $m/s^2/N$ to approximately 250 $m/s^2/N$. The Y-axis of the compliance graph was set to view from -1.8E-05 m/N to 0 m/N. With the graphs set up in this manner, accelerance was used to observe the presence of both the skin peak and the bone peak while compliance was used to observe non-ideal peaks to the left of the bone peak.

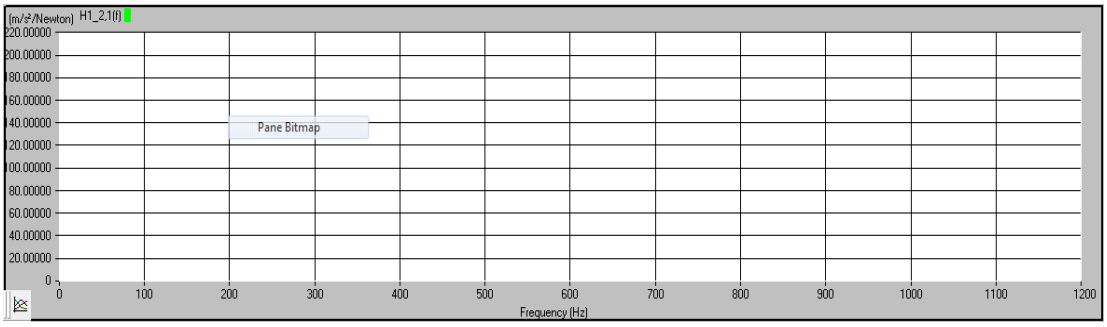

Fig. 58 (above)
RT Pro graph setup for accelerance

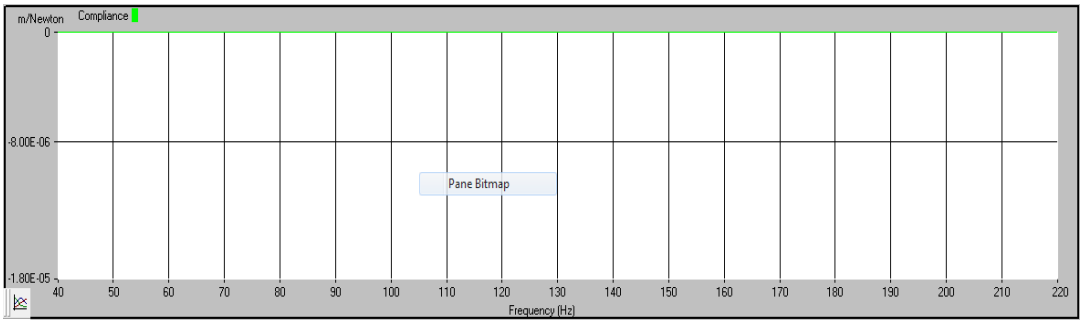

Fig. 59 (above)
RT Pro graph setup for compliance

Some noise is expected to appear on the FRFs during data collection, but the small peaks in compliance seemed to be exceptionally large (amplitude greater than -8.00E-06 m/N) in data sets that deviated from measurements made by QMT **(Fig. 60)**. When these peaks had lower amplitudes (i.e., less than -8.00E-06) MRTA measurements had decreased deviation from QMT.

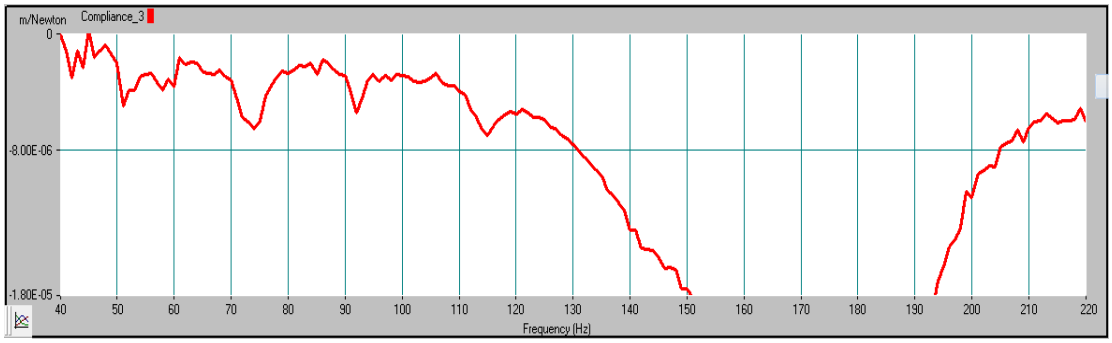

Fig. 60
Narrowed compliance FRF for artificial ulna raw data showing bone peak (right) and the region before it. Notice that there are no peaks besides the bone peak below the midline on the Y-axis (-8.00E-06 m/N),

Data collection began by opening up RT Pro, pressing the initialize button, the start button, and the start source button in that order. After about thirty seconds, random noise averaged out and a clear waveform gradually formed. The frequency of the middle of the skin peak was identified, and if it was not between 510-580Hz, the hand crank of the linear module was used to increase or decrease the static load. After adjusting the crank, the "stop" button was clicked on RT Pro and then data collection was re-initialized. This process was repeated until the skin peak was in the correct frequency range.

After aligning the skin peak, the accelerance graph of the data **(Fig. 61)** was observed to ensure that there were no large extra peaks visible. If extra peaks were visible in accelerance, the probe was lifted and the ulna was removed and realigned. During realignment the blue strap was checked for tightness and the ulna was checked for stability.

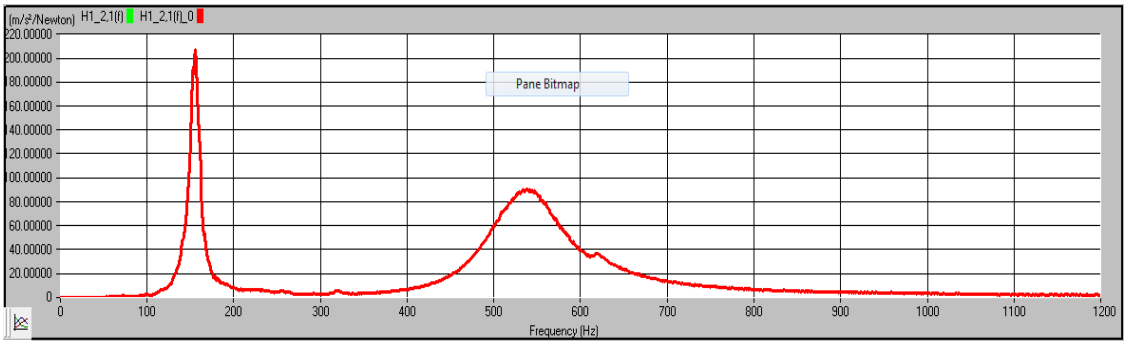

Fig. 61
Accelerance FRF for artificial ulna raw data

Once the skin peak and accelerance graph were acceptable, the compliance FRF was observed to see if any peaks fell below the -8.0E-06 line. If so, several techniques were used to decrease their amplitude. After shutting off the excitation and data collection, the probe was raised and moved transversely across the ulna in the Y direction. Data collection was restarted and RT pro was observed to see if the amplitude of extra peaks had decreased. The probe was incrementally moved across the ulna and peaks in compliance were checked for amplitude until all of the peaks were above the -8E-06 m/N line or until the probe had crossed to the lateral side of the posterior border with one third of it not contacting the ulna.

If the probe had been incrementally moved in the Y-direction and amplitude of compliance peaks left of the bone peak were still below the -8E-06 m/N line, the probe

was raised and the ulna was adjusted. The ulna was adjusted based on the frequency of the peaks with amplitudes beyond the line in compliance. Typically, there were three frequency ranges that often had peaks surpass the -8E-06 m/N line: 70-80 Hz **(Fig. 62)**, 90-100 Hz , 110-125 Hz. Peaks in the 70-80 Hz region usually indicated that the proximal end of the ulna needed to be rotated slightly downward around the curvature of the trochlea. Peaks in the 90-100Hz and 110-125Hz regions usually indicated that the proximal end of the ulna needed to be rotated upward around the curvature of the trochlea. While peaks that were separate from the bone peak in this region **(Fig. 63)** usually indicated a need for readjustment, inflections on the side of the bone peak **(Fig. 64)** did not cause the same degree of difference from QMT measurements and no adjustment was needed In both cases, the rotation was very slight and was rarely greater than 3mm of movement. The stability of the ulna was checked after it was rotated.

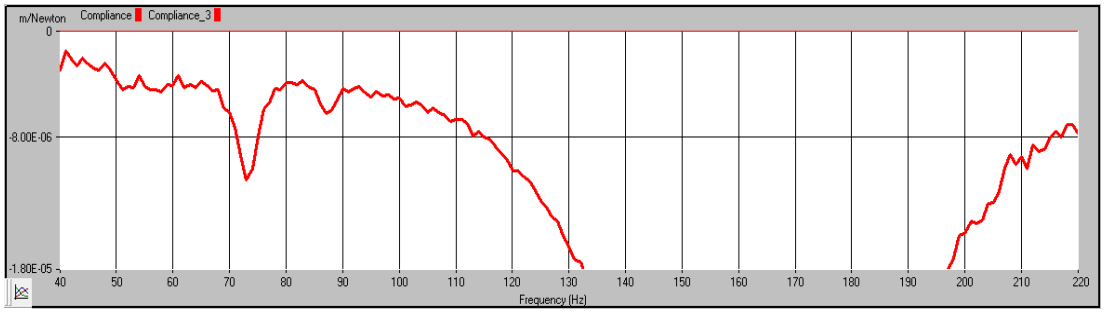

Fig. 62
Narrowed region of compliance graph showing a peak at 74Hz that crosses the midline on the Y-axis.

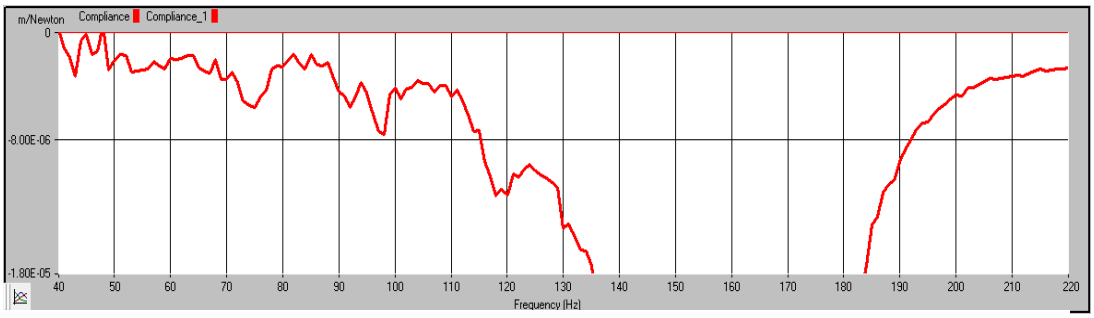

Fig. 63 (above)
Narrowed region of compliance graph showing a peak at 118Hz that crosses the midline on the Y-axis and is completely separate from the bone peak.

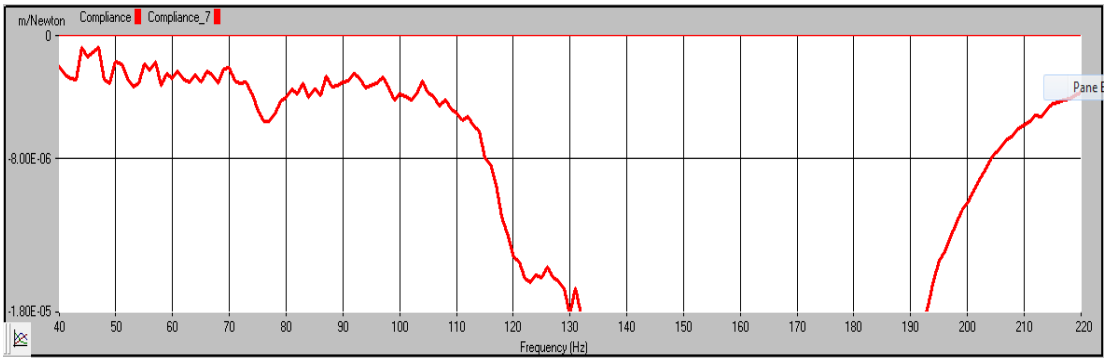

Fig. 64
Narrowed region of compliance graph showing a peak at 123Hz that crosses the midline on the Y-axis and is not entirely separate from the bone peak.

The probe was then lowered in intentional misalignment medial to the posterior border again and the data collection was restarted as previously described. The ulna rotation and probe placement was repeated until the peaks in compliance had decreased in amplitude. After the peaks had decreased, data collection was stopped and the four screws around the upper stage of the MRTA device were tightened. Collection was restarted and the compliance FRF was observed again. If all of the extra peaks in compliance still had decreased amplitude, then data was collected for up to 150 frames and saved. Three measurements of 150 frames were made consecutively for a sample. In some cases, tightening the screws on the test frame

around the linear module increased the amplitude of the peaks beyond the -8E-06 m/N line, and the screws had to be loosened and remain loose during data collection.

Typically, collection of one sample took thirty-five to sixty minutes. A minimum of three such samples from each artificial ulna was taken during three different time periods with the ulna dismounted and removed from the MRTA device between samples.

Data Analysis

QMT

QMT 3-point bending force and displacement data were analyzed by Testworks 4 software accompanying the MTS Q-Test Elite Mechanical Testing System. This software calculated K_b as the best-fitting slope of the force/displacement (i.e., Load/Crosshead) curve in the same force range in which MRTA data are collected as seen in (**Fig. 65**). K_b was then used to calculate EI. The calculated EI value for each ulna was reported as the average of three separate trials, with the ulna dismounted between each trial.

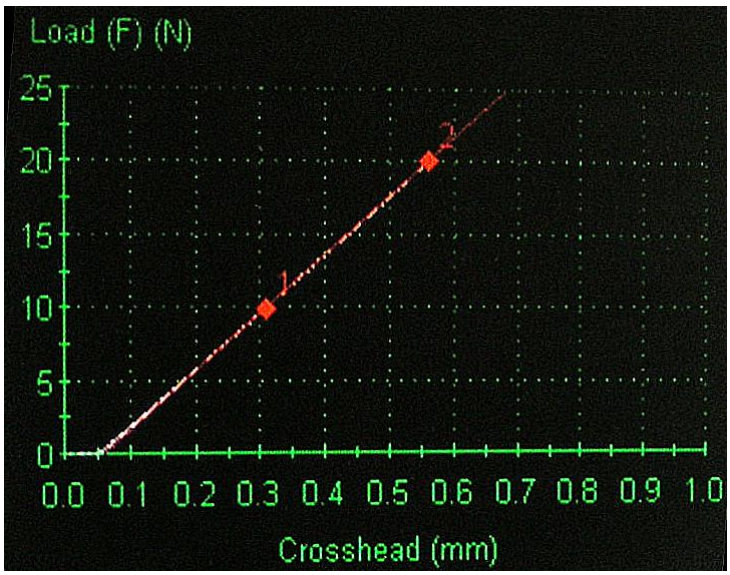

Fig. 65
Screenshot of QMT data collected using MTS Testworks 4 software. Bending stiffness (in units of N/mm) is calculated as the slope of the data between points 1 and 2.

Bending strength data was derived from the force/displacement curve recorded during the fracture loading cycle. Fracture force was recorded as the highest force before the ulna broke (indicated by the sudden drop in load in the QMT data) **(Fig. 66)**.

Previously published MRTA data relating strength and stiffness had plotted scaled maximum load vs. EI (29). As mentioned above, scaled maximum load adjusts the maximum force to account for variations in test conditions, i.e., anterior posterior diameter and span of support. Therefore, scaled maximum load was calculated for the fracture data collected in this study in order to compare it to data from previous studies on monkey tibias and cadaveric human ulnas**(**29, 14**).**

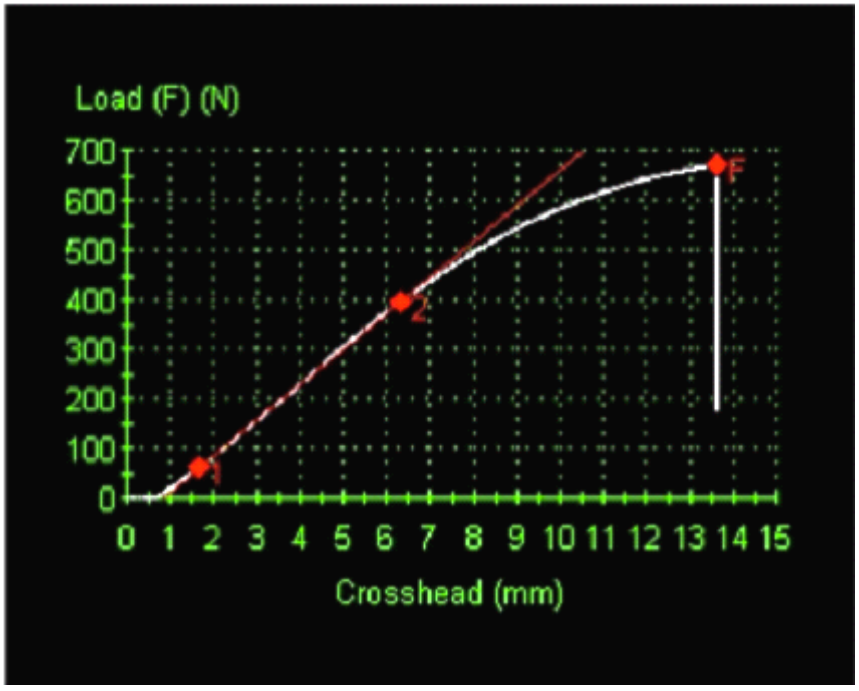

Fig. 66
Screenshot of QMT data collected using MTS Testworks 4 software. Bending strength (in units of N) is calculated as the highest force before the ulna breaks, indicated by the sudden drop in load.

MRTA

MRTA 3-point bending data were analyzed by Ohio University's proprietary Matlab program, aeiou.m. This program converted each complex accelerance FRF into the corresponding complex stiffness (force/displacement) and complex compliance (displacement/force) FRFs. These were then fitted to the corresponding analytical FRFs derived from the differential equations of motion for a 7-parameter mathematical model of the mechanical skin-bone system to estimate the ulna's antero-posterior bending stiffness K_b **(Fig 67)**. From K_b, EI was calculated using the Euler beam solution for a simply supported beam.

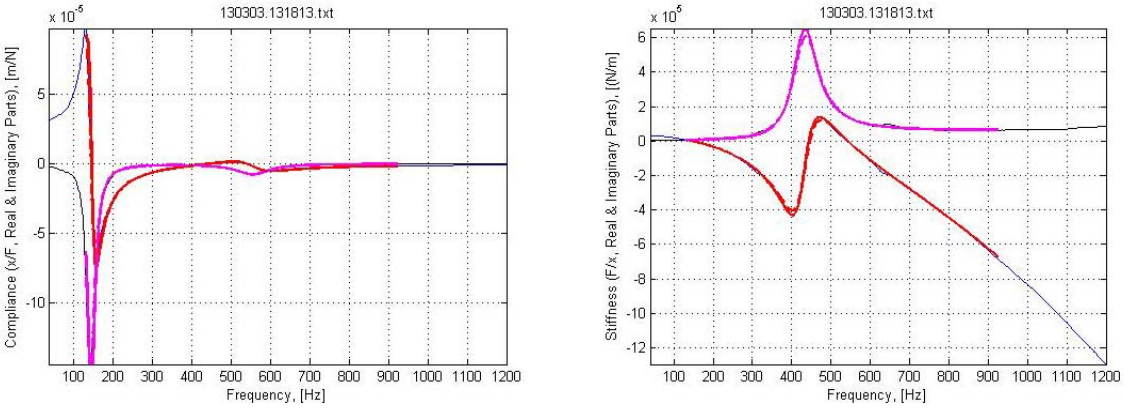

Fig. 67
Complex compliance (left) and stiffness (right). Raw data is represented by blue and black lines. Red and pink lines represent the mathematical fit to the data.

The program aeiou.m estimates for each of the seven parameters in the model by fitting the model to the calculated compliance and stiffness FRFs. The parameter estimates derived from compliance and stiffness FRFs differed from one another. Additionally, data were collected from 40-1200Hz, but many different frequency ranges can be used to fit the 7-parameter model to the FRFs (e.g from 100Hz to

800Hz). The parameter estimations derived from the various frequency ranges also differ from one another. To decide which parameter estimates to report, aeiou.m chooses the frequency range that minimizes the root mean square (RMS) of the pair-wise differences between the seven parameter estimates derived from the stiffness and compliance FRFs. Then the average of the estimations of K_b from the compliance and stiffness FRFs derived from the frequency range with the lowest RMS is used to calculate EI. In this project, EI was only recorded when RMS was less than 20% and the fitted frequency range included all of the bone peak and skin peak.

Statistical Analysis

The association of ulna flexural rigidity measured by MRTA and QMT was determined by regression analysis. Then, EI measurements made by MRTA and made by QMT were individually associated with the scaled maximum load measured by QMT during bending strength tests.

The EI value for each ulna was reported as the average of three trials. For MRTA, each trial consisted of three measurements and for QMT measurements were collected until the internal coefficient of variation (CV) (standard deviation/average) of the last five measurements taken was less than 1%. For each sample, the standard error, standard deviation, and within trial CV were calculated. For each ulna, the average of all samples collected was calculated. Standard deviation, standard error, and between trial CV were calculated for the average of all samples for each ulna.

Precision was calculated as the within-trial CV of EI calculated from three MRTA FRFs (one trial) and five QMT load/displacement curves (one trial), collected without dismounting the ulna from the humerus. Repeatability was calculated as the between-trial CV from all trials collected by each device from each one of the ulnas, with dismounting of the ulna from the humerus between trials.

Bland-Altman analysis was used to determine the bias and limits of agreement between measurements of ulna bending flexural rigidity measured by MRTA and QMT. Analysis of the limits of agreement quantified levels of fixed and proportional bias as well as the range of random variation in measurement differences. A fixed bias between methods was detected by single sample, two-sided t- tests. Proportional bias was detected by regression analysis.

For clinical interchangeability, differences between measurements by two methods should be within 10% to avoid clinical misinterpretation. Based on the average repeatability of measurements of ulna flexural rigidity with Ohio University's MRTA (3.1%) and QMT (1.6%) instruments, the number of ulnas used in this project was sufficient to detect a 10% fixed bias and a 10% proportional bias between methods with 5% probabilities of Type 1 and Type 2 errors, respectively.

RESULTS

Sawbones Dimensions

Artificial ulnas were received in four different batches, chronologically named Batch 1, Batch 2, Batch 3, and Batch 4. The bones were weighed after they were received. Mass increased with glass fill, but ulnas within each level of glass fill varied in mass, indicating some manufacturing variation **(Fig. 68).**

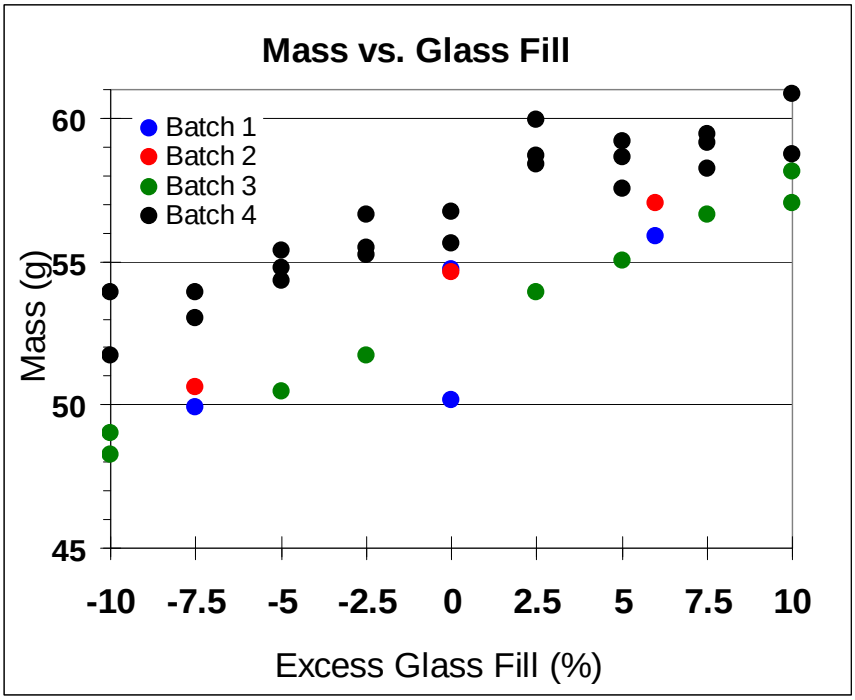

Fig. 68
Graph showing variation in mass within each increment of glass fill.

Measurements of EI from QMT and MRTA were also plotted against glass fill. Like mass, EI increased with glass fill, but was not constant for all ulnas within each level of glass fill. There was also manufacturing variation in the stiffness of the ulnas. Despite this variation, ulnas were still produced within the physiological range of EI in women, $10Nm^2$ to $27Nm^2$. Both methods of measuring EI showed the same variation.

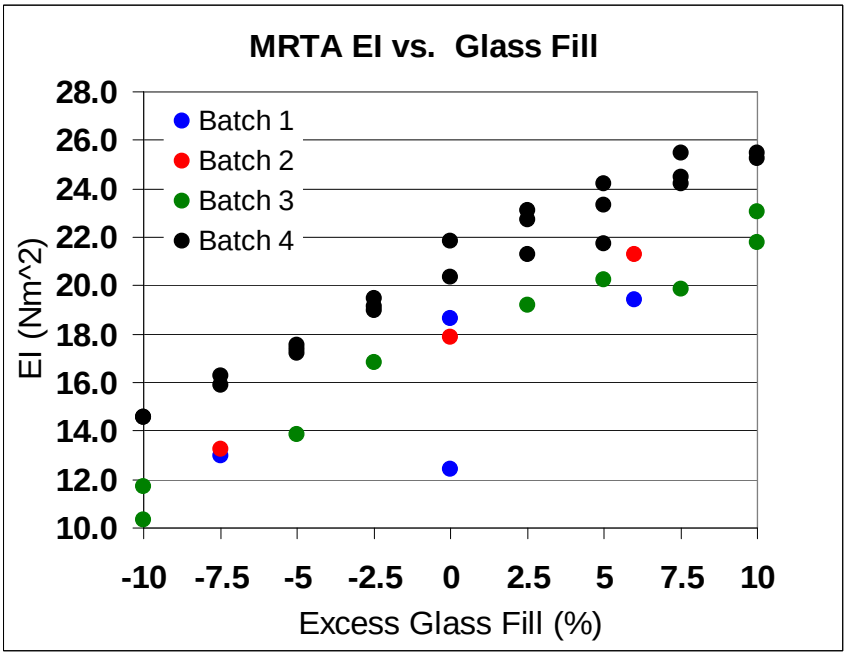

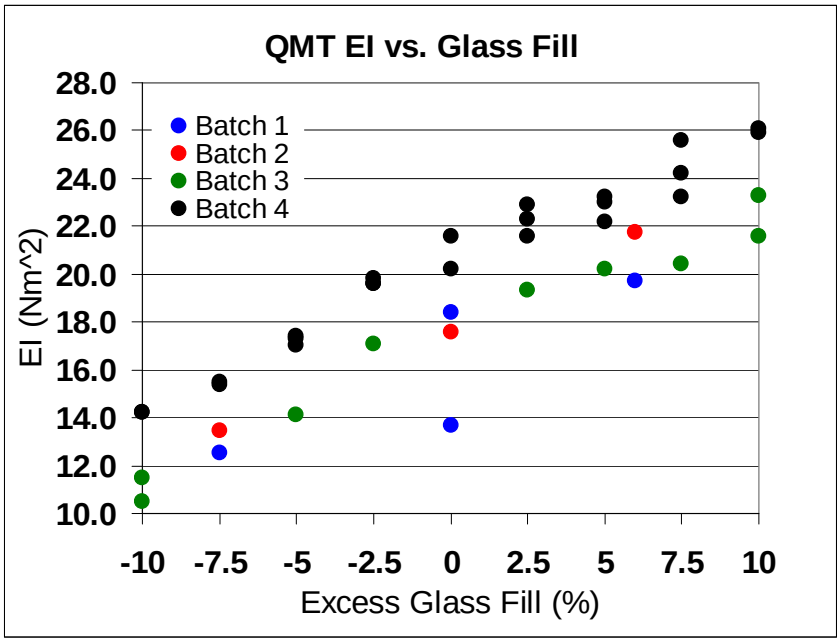

Fig. 69 (top) and 70 (bottom)
Measurements of EI by MRTA (top) and QMT (bottom) revealed that ulna EI varied within each level of excess glass fill.

Reproducibility of EI Measurements

MRTA precision (1.0 ± 1.0%) and repeatability (3.1 ± 3.1%) were not as high as those of QMT (0.2 ± 0.2% and 1.3 + 1.7%, both $p<10^{-4}$)) **(Table 2)**. The precision and repeatability of QMT is very good, as would be expected for a gold standard reference method. Despite being not as high as QMT, MRTA measurements of precision **(Fig. 71)** and repeatability **(Fig. 72)** would be sufficient for clinical use, e.g., detecting effects of treatment over a short period of time.

Reproducibility			
Method	**Precision**	**Repeatability**	**P-value**
QMT	0.2 ± 0.2%	1.3 + 1.7%	$p<10^{-4}$
MRTA	1.0 ± 1.0%	3.1 ± 3.1%	$p<10^{-4}$

Table 2 (above)
Reproducibility (precision and repeatability) measurements by each method

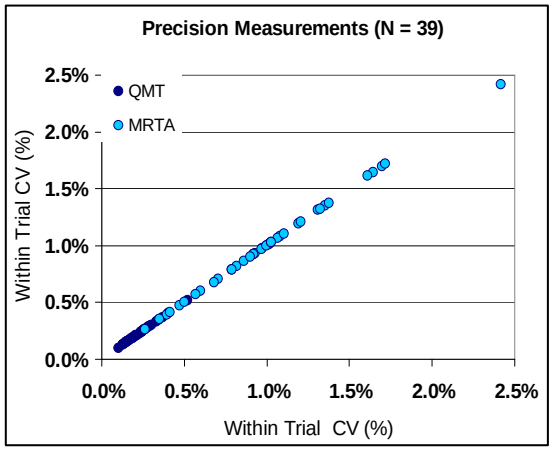

Fig. 71
Comparison of precision of QMT and MRTA

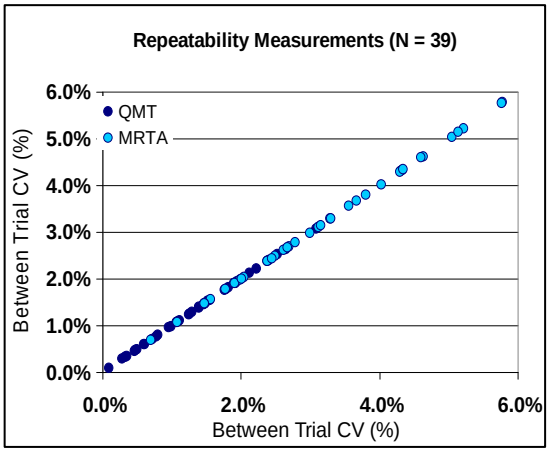

Fig. 72
Comparison of repeatability of QMT and MRTA

Regression Analysis of EI Measurements

Regression analysis (**Fig. 73)** found a very strong association between MRTA and QMT measurements of EI, MRTA = 1.001 × QMT (R^2=0.999).

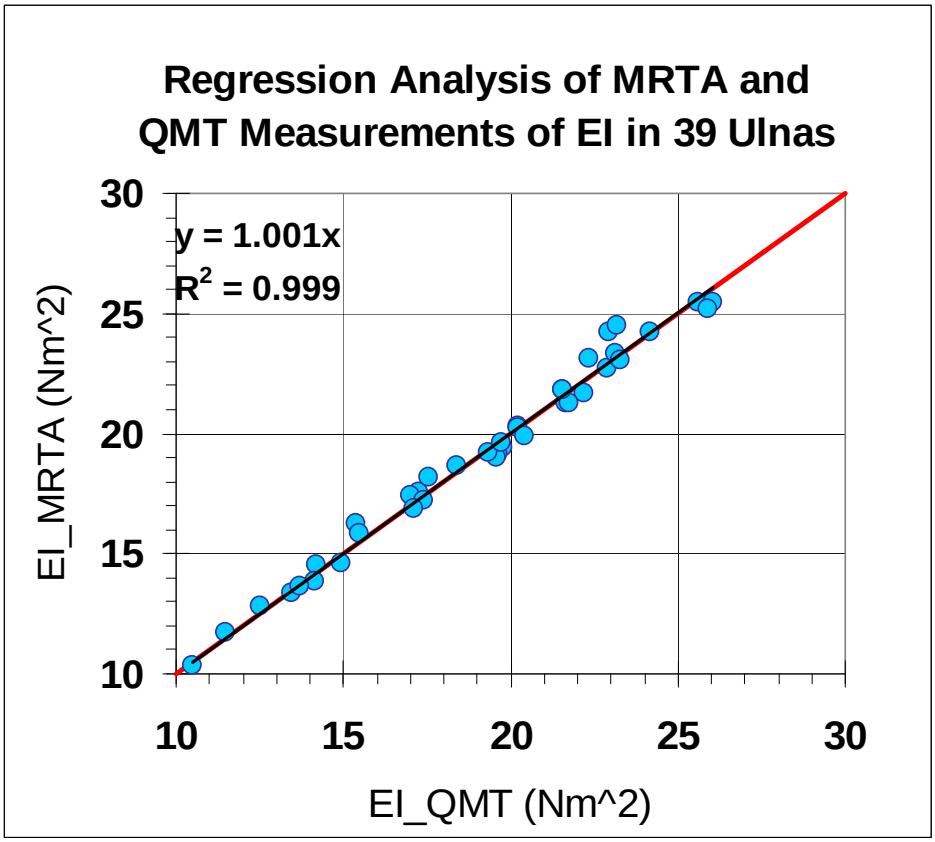

Fig. 73
Regression of EI measured by MRTA on paired measurements by QMT (N = 39). Red line = identity line . Black line = regression line: y = mx + b. m = 1.001 ± 0.004, $p<10^{-63}$; b ≡ 0, p = 0.44.

Bland-Altman Analysis of EI Measurements

Bland-Altman analysis (**Fig. 74)** showed that MRTA was unbiased (mean difference = 0.2 ± 0.8%, p=0.67) with respect to QMT. Individual MRTA and QMT measurements were interchangeable within limits of agreement ±5%, as determined by

the 95% confidence interval of individual measurements. The 95% confidence interval on the limits of agreement ranged from ±4% to ±6%.

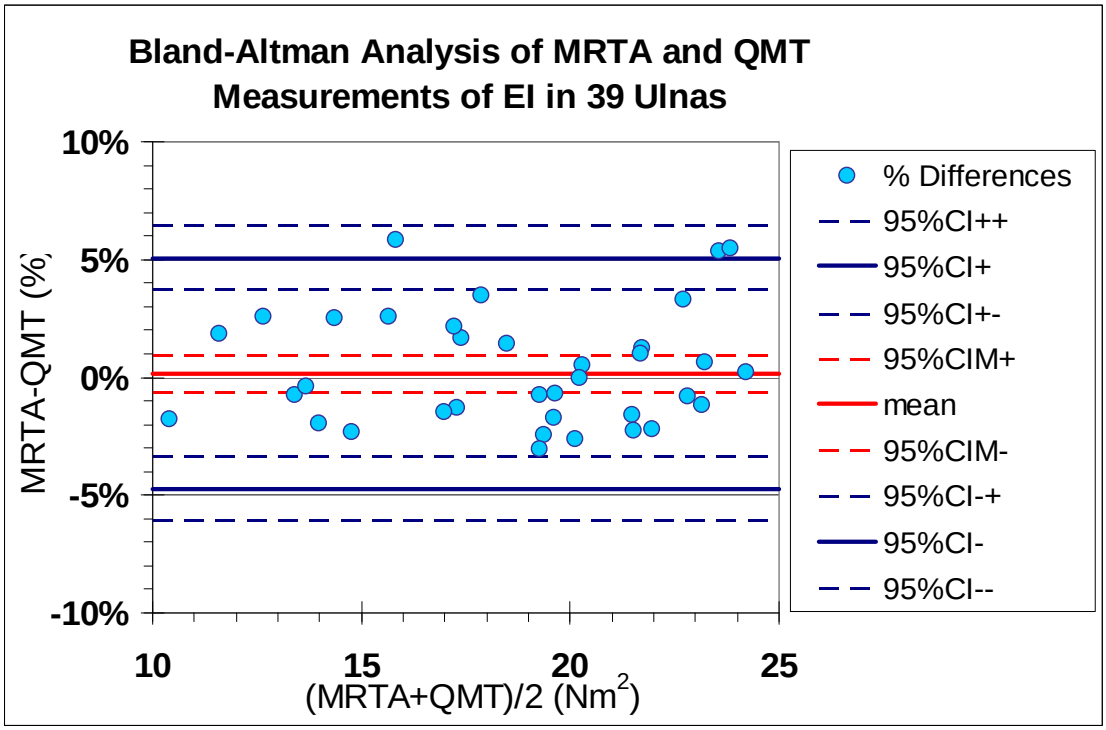

Fig. 74
Bland-Altman analysis of paired measurements of EI by MRTA and QMT in the same ulnas. 95%CIM = confidence interval of the mean difference. 95%CI = confidence interval of individual paired differences.

Relationship between Bone Stiffness and Strength in Artificial Ulnas

Regression analysis found that the relationship between QMT measured stiffness and QMT measured strength in the first eight ulnas tested **(Fig. 75)** was not as strong ($R^2 = 0.79$) as previously reported data ($R^2 = 0.98$) (29). However, when the bending strength tests were separated by batches **(Fig. 76,** the four ulnas in Batch 4 showed a very strong (R^2=1.0) relationship.

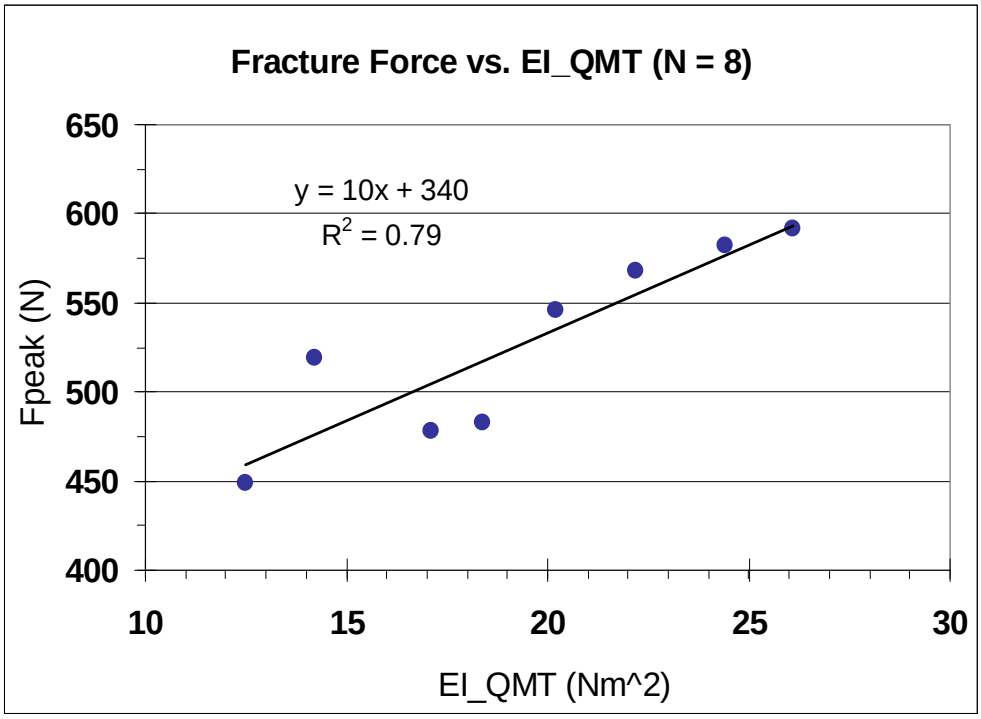

Fig. 75 (above)
Regression analysis of bending strength (fracture force) vs. EI measured by QMT for the first eight ulnas measured.

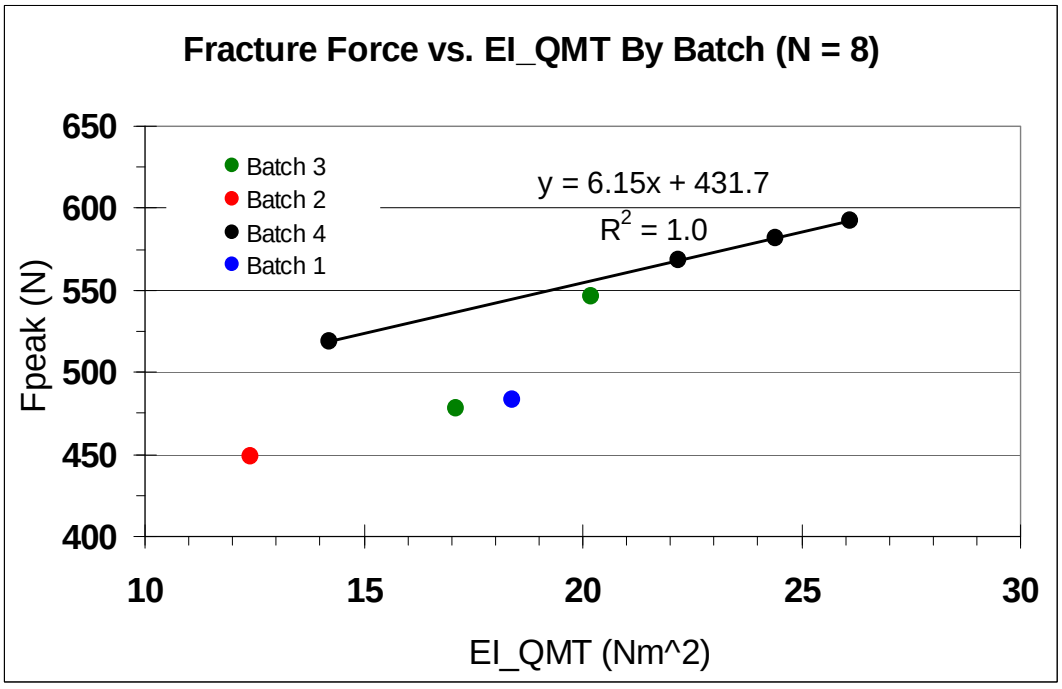

Fig. 76
Regression analysis of bending strength (fracture force) vs. EI measured by QMT separated by batch for the first eight ulnas measured.

To determine whether or not there was a batch effect on the stiffness and strength relationship, three additional ulnas were tested from Batch 4 and one additional ulna was tested from Batch 3. Despite the three ulnas in Batch 3 showing a strong association between stiffness and strength measurements ($R^2 = 0.98$), the larger sample size from Batch 4 (N = 7) showed a very weak relationship ($R^2 = 0.22$) **(Fig. 77)**.

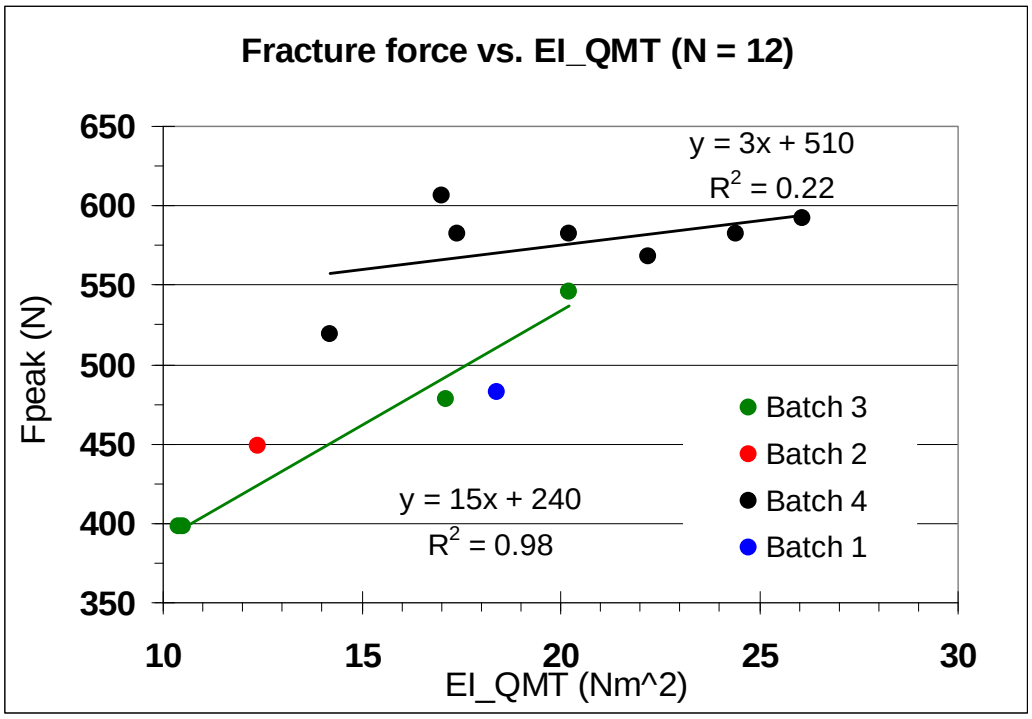

Fig. 77
Regression analysis of bending strength (fracture force) vs. EI measured by QMT separated by batch for the first twelve ulnas measured.

Three ulnas were then measured using the test setup with a shortened humerus described previously. These ulnas still showed a weaker relationship ($R^2 = 0.78$) than previously published studies **(Fig. 78)**.

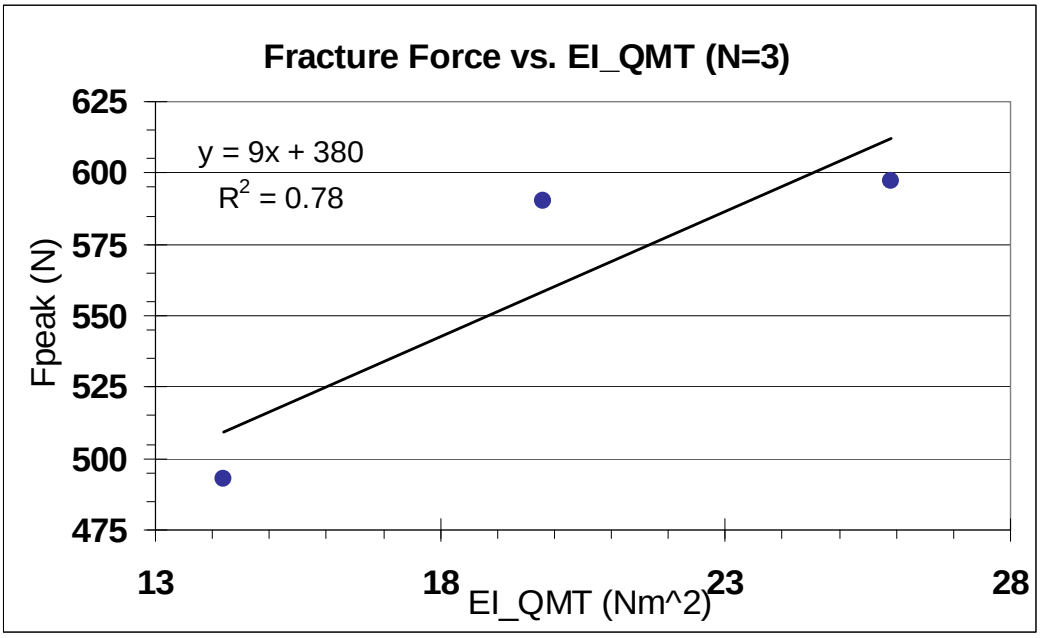

Fig. 78
Regression analysis of bending strength (fracture force) vs. EI measured by QMT separated for three ulnas measured with the new setup.

The relationship between bending stiffness and strength for all fifteen ulnas measured was much weaker ($R^2 = 0.59$) **(Fig. 80)** than the previously published relationship Moreover, the regression analysis for all fifteen ulnas found a substantial and statistically significant non-zero y-intercept of 340N, indicating that 340N would be needed to fracture an ulna with zero stiffness. Such a non-zero y-intercept on a strength vs. stiffness graph is physically unrealistic for any material.

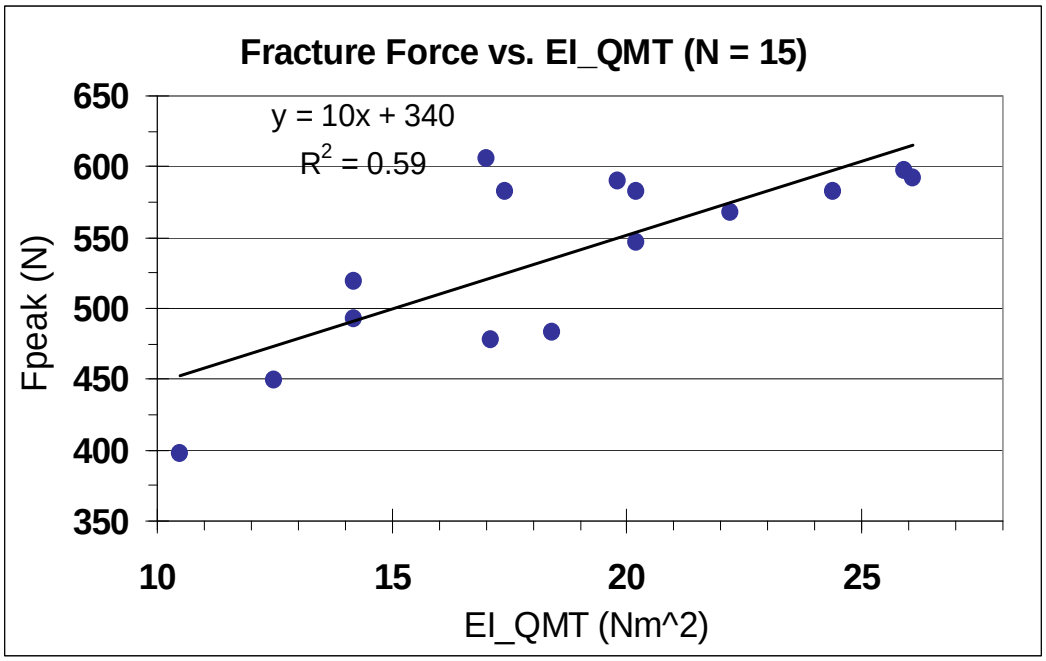

Fig. 80
Regression analysis of bending strength (fracture force) vs. EI measured by QMT separated for all ulnas measured for strength in this study.

Scaled maximum load adjusts the fracture load to account for different spans of support and different anterior posterior diameters in specimens under test. Therefore, scaled maximum load was also calculated for the fracture data collected in this study in order to compare these data to data from previous studies on monkey tibias and cadaveric human ulnas (**Fig. 81) (**29, 14**).** The results were similarly unrealistic due to the presence of a statistically significant non-zero y-intercept.

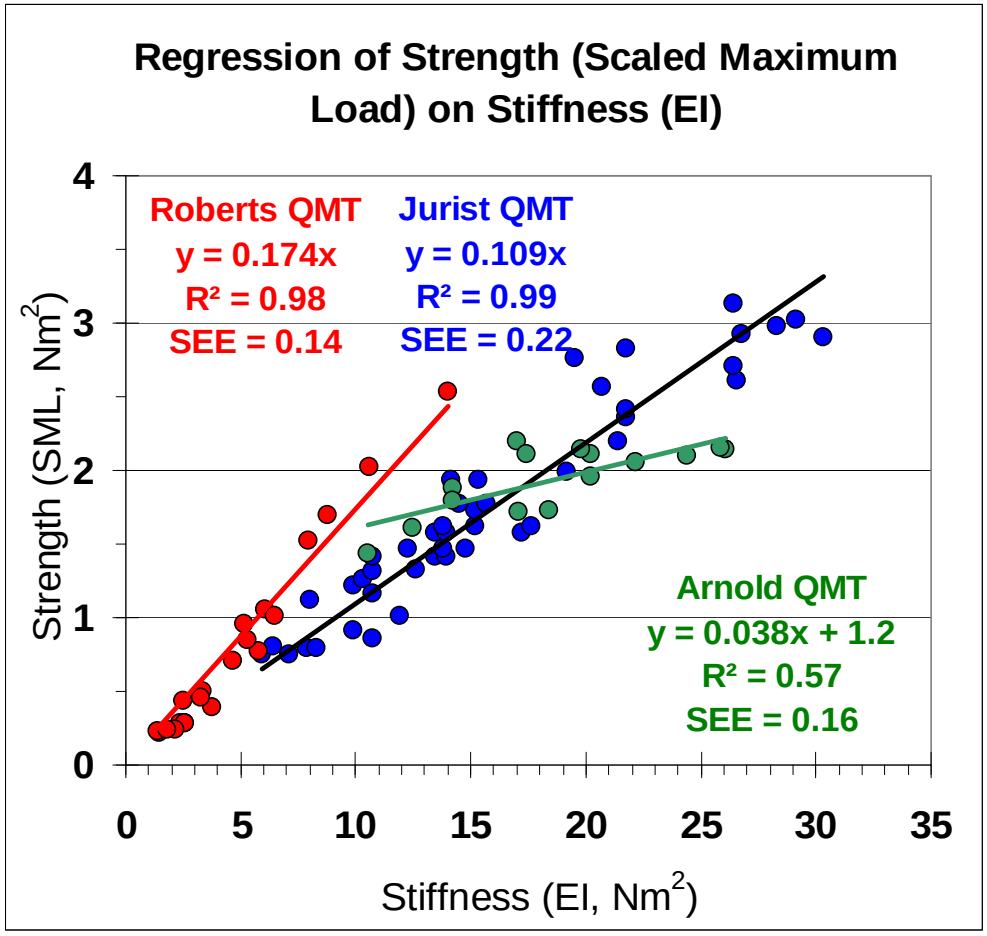

Fig. 81
Regression analyses of QMT measurements of bending strength as scaled maximum load and QMT measurements of EI. "Roberts" refers to data from excised monkey tibias (29). "Jurist" refers to data from embalmed human cadaveric ulnas (14). "Arnold" refers to data in the present study from artificial human ulna bones with biologically unrealistic diameters. SEE = Standard error of the estimate.

Typically, increases in bone stiffness and strength tend to be accompanied by increases in anterior posterior diameter. However, the artificial ulna bones used in this study had been manufactured to increase stiffness without variation in anterior posterior diameter. Manufacturing variation in the diameter of the artificial human ulnas had been only 1%. This was biologically unrealistic compared to the 81%

variation in anterior posterior diameter reported in human cadaveric ulnas (14). Therefore, the scaled maximum loads for the fifteen artificial human ulnas fractured in this study were adjusted to reflect a more biologically realistic 81% variation in diameter in proportion to their relative maximum loads. That is, the scaled maximum load of the ulna with the highest maximum load was scaled up by 81% compared to the scaled maximum load of the ulna with the lowest maximum load, and the scaled maximum loads of the other fractured ulnas were interpolated proportionally.

This adjustment produced a stronger relationship ($R^2 = 0.98$) between scaled maximum load and EI measured by QMT **(Fig. 82)**, and between scaled maximum load and EI measured by MRTA ($R^2 = 0.97$) **(Fig. 83)**. The slope of the regression line relating scaled maximum load and EI for embalmed cadaveric human ulnas was not significantly different from the slope of the regression line for the artificial human ulnas with EI measured by QMT (cadaveric = 0.109 ± 0.002, artificial = 0.115 ± 0.005, $p = 0.19$) or MRTA (cadaveric = 0.109 ± 0.002, artificial = 0.116 ± 0.005, $p = 0.12$).

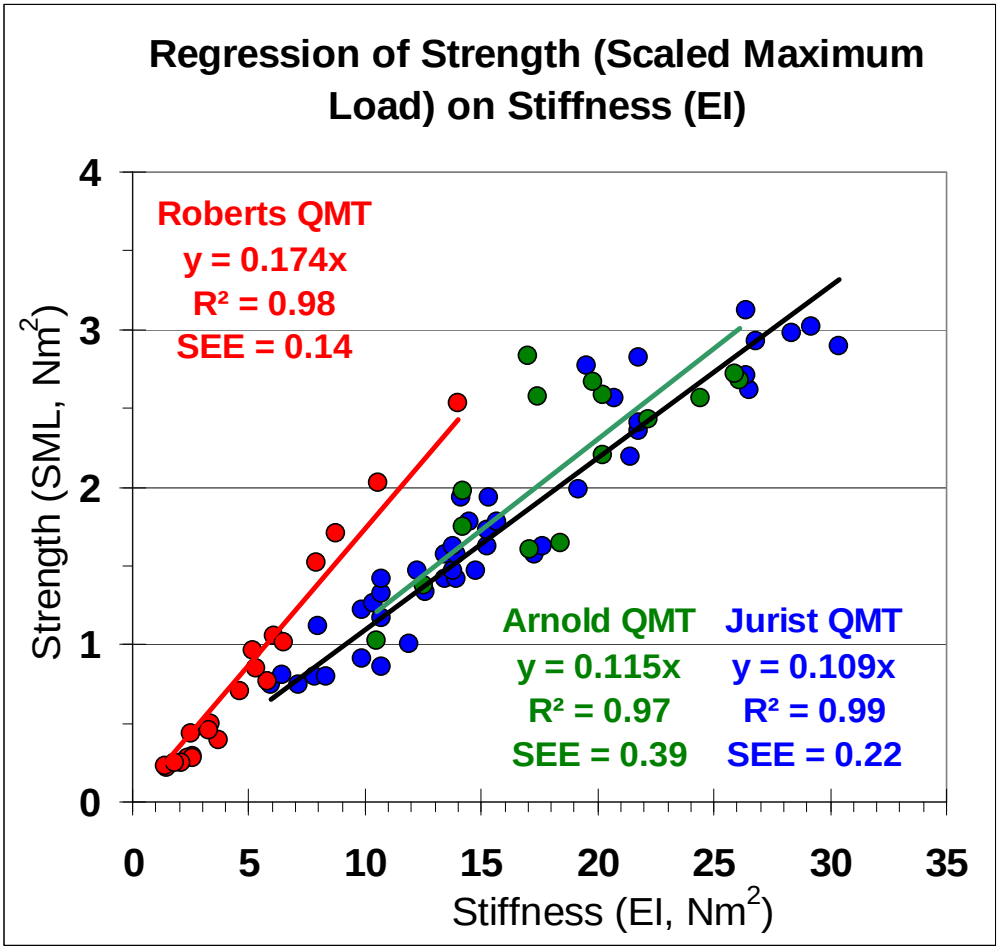

Fig. 82
Regression analyses of QMT measurements of bending strength as scaled maximum load and QMT measurements of EI. "Roberts" refers to data from excised monkey tibias (29). "Jurist" refers to data from embalmed human cadaveric ulnas (14). "Arnold" refers to data in the present study from artificial human ulnas, with data points adjusted for a more biologically realistic 81% variation in ulna diameter. SEE = Standard error of the estimate.

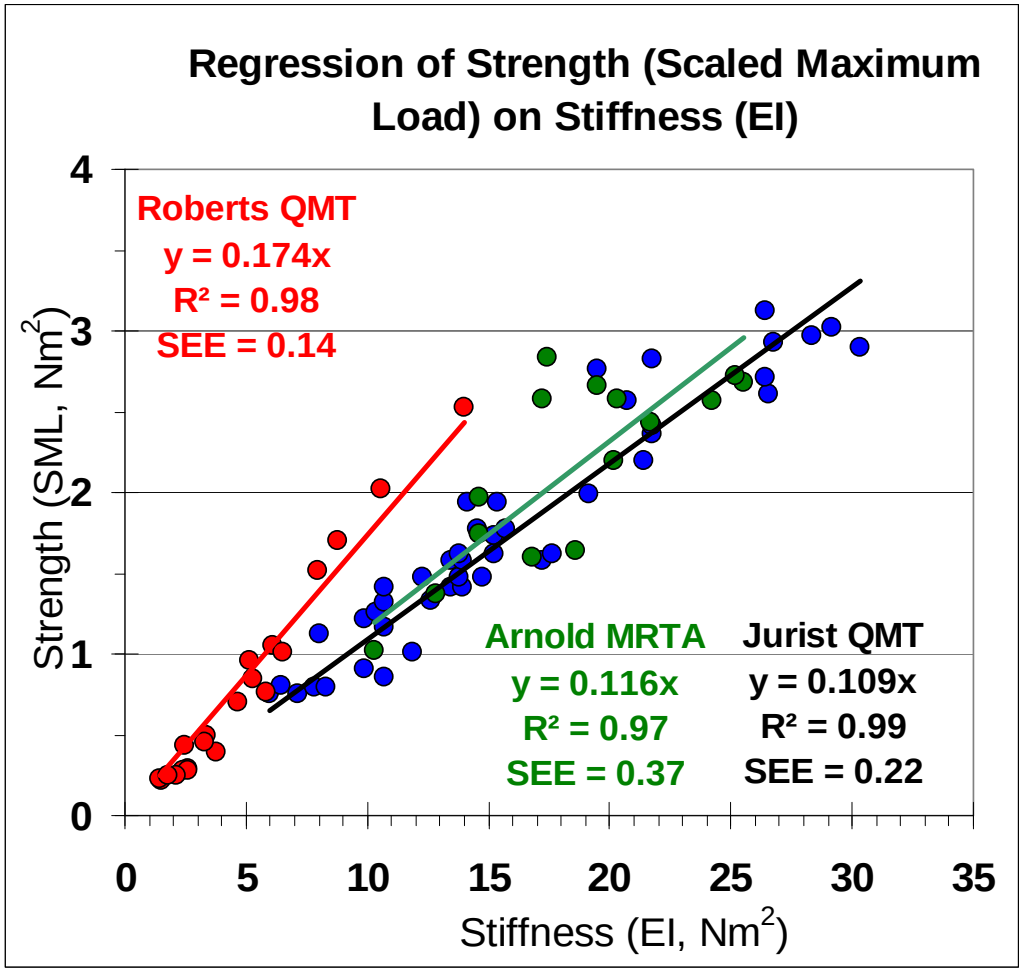

Fig. 83
Regression analyses of QMT measurements of bending strength as scaled maximum load and measurements of EI. "Roberts" refers to data from excised monkey tibias with EI measurements made by QMT (29). "Jurist" refers to a study on embalmed human cadaveric ulnas, with EI measurements made by QMT (14). "Arnold" refers to the present study on artificial human ulna bones with EI measurements made by MRTA and data points adjusted for an 81% variation in ulna diameter. SEE = standard error of the estimate.

DISCUSSION

This project set out to validate Ohio University's MRTA device through association with QMT measurements of bending stiffness and bending strength in artificial human ulnas. This study was strengthened by controlling potential sources of error prior and during data collection. However, this study is also weakened by other sources of error that were not controlled.

Strengths

This study was able to exhibit control over several possible sources of error. First, physiological measurements of EI could be measured in artificial human ulnas despite many differences between artificial and *in vivo* ulnas. *In vivo* forearms are attached to the distal humerus via a joint capsule with ligaments and fat pads, whereas this study simply placed the ulna on the humerus. Undoubtedly, ulnas were placed on the humerus and steel block in variable orientations during trials of data collection. However, this study overcame a large portion of variation in ulna placement on the humerus by viewing the trochlea as a clock face and aligning the tubercle of the coronoid process of each ulna up with the nine o'clock position. Markings on each ulna also standardized placement on the humerus between trials.

The artificial human ulnas represent excised bones could not replicate *in vivo* conditions. Nevertheless, the artificial human ulnas were useful models for validating MRTA measurements of EI in this project when they were wrapped in tourniquet rubber that imitated skin and soft tissue.

W Another source of error in this project could have been variation in the static preload applied to each ulna during MRTA data collection. This possible source of error was minimized by adjusting the static preload so as to locate the "skin peaks" in the accelerance FRF of each ulna within the same narrow frequency range during data collection.

Weaknesses

Confidence in this study should be tempered by an awareness of its limitations. Previous studies on bones produced by Pacific Research Laboratories/Sawbones® have shown the mechanical properties of artificial tibiae, femurs, and humeri to have values in the range of human bone. Despite manufacturing variations in mass and EI, the artificial human ulnas were still useful models for validating MRTA measurements of EI against QMT because their range of EI fell within the range of ulna EI in the human population. However, the artificial human ulnas could not be manufactured to span the entire range of EI that we have measured in human subjects. Previously published data from legacy MRTA devices(32) and unpublished *in vivo* studies with Ohio University's MRTA device have found EI values ranging up to 120 Nm^2 in men, which are well above the highest EI (27 Nm^2) measured in Sawbones® ulnas in this project . It is unknown if the measurement precision, repeatability, and accuracy determined in this study would still apply to ulnas with EI of 120 Nm^2 or higher.

An additional weakness of this study was that all data collection was conducted by one technician, who may have been subject to technician bias. It remains undetermined if other technicians would collect data with similar results.

Another weakness of this study is the lack of a satisfactory theoretical explanation for the observed need to adjust the scaled maximum load of artificial ulnas for the range of diameter in embalmed human ulnas in order for the scaled maximum loads of the artificial ulnas to span a similar range of scaled maximum load as excised monkey tibias (29). Nor is it known why the scaled maximum load of the embalmed ulnas did not need to be adjusted for their range of diameter in order for their scaled maximum loads to span a similar range of scaled maximum load as excised monkey tibias (14, 29). It is not even known whether the scaled maximum loads of monkey tibias and embalmed and artificial human ulnas should be expected to span the same range. Nor is it known why the scaled maximum load of the artificial human ulnas had an apparently physically unrealistic significant y-intercept without this adjustment. More data on scaled maximum load and flexural rigidity in other long bones would need to be compared in order to gain better insight into this issue.

Technical Advances

Reproducibility

This was the first study to report a direct comparison of the reproducibility of MRTA and QMT measurements of EI. Previously published studies have estimated repeatability of QMT three-point bending tests of rat femora based on paired

measurements of stiffness and strength in contralateral limbs to be 7-15% in stiffness measurements and from 4-5% in strength measurements (13, 18). Additionally, QMT compression tests of artificial tibias and femora have reported a repeatability of 6% (12). The present study made repeated measurements of artificial ulna EI by QMT in repeated trials to determine precision and repeatability on the same artificial human ulnas over the same range of applied load. Although it was not possible to estimate QMT measurement repeatability in the bending strength tests, the 1.3% QMT repeatability of EI measurements in this study conformed more closely to expectations for a gold standard reference method than the previously reported values.

The 1.0% MRTA measurement precision and 3.1% repeatability found in this study are the best measures of MRTA reproducibility reported to date. Using artificial ulnas as experimental specimens undoubtedly contributed to these improved levels of precision and repeatability, as previous studies have been based on measurements *in vivo.* For example, legacy MRTA devices on *in vivo* human forearms were reported to range in precision from 2.9% to 4.3% and to achieve a repeatability of 5.3% (20, 24, 23, 16, 32). It must be acknowledged that artificial ulnas are not inclined to move during a data collection as *in vivo* arms are. In addition, artificial ulnas do not experience mechanical loading that might affect EI between trials as *in vivo* arms may do. Nevertheless, the improved reproducibility of EI measurements by MRTA in this project cannot be attributed entirely to the use of artificial ulnas, because an observational study recently conducted with the same OU MRTA system found *in vivo* precision and repeatability to be 1.8% and 3.5%, respectively (1).

Accuracy of EI Measurements

This was only the second investigation of the accuracy of an MRTA device. **Fig. 84** compares the regression analysis of MRTA and QMT measurements of EI in this study to the previously reported Stanford University study in monkey tibias (29). Despite having a strong relationship between MRTA and QMT measurements, Stanford's MRTA data were far from the identity line.

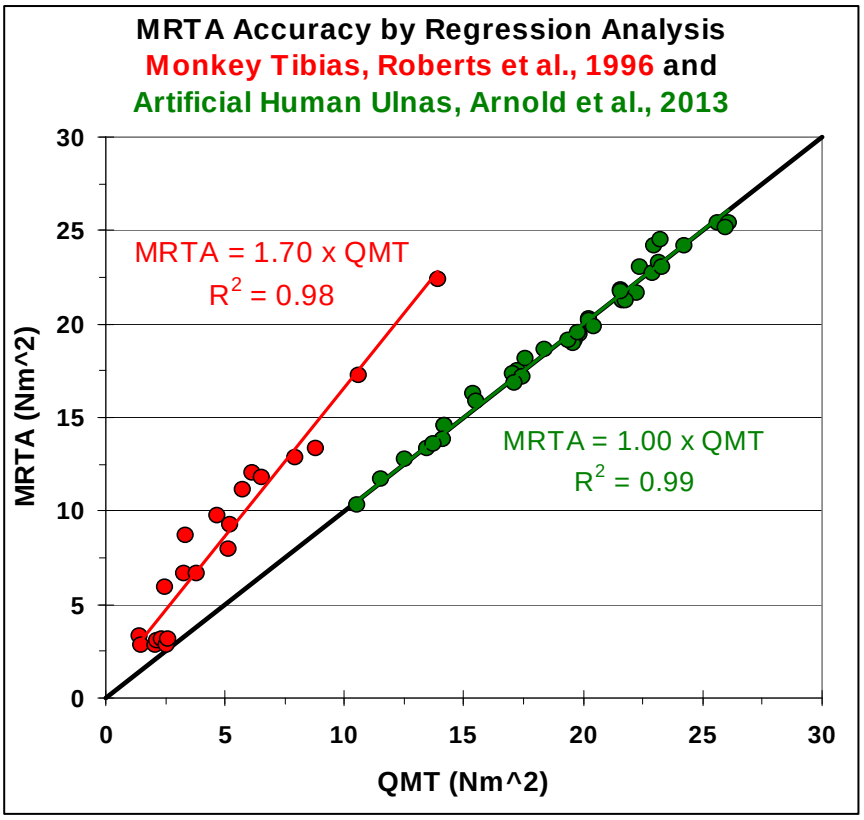

Fig. 84
Regression analyses of MRTA QMT measurements of EI. The red data are from the previous Stanford University study and the green data are from the present study.

Fig. 85 compares the Bland-Altman analyses of paired measurements of EI from MRTA and QMT in the present study to the corresponding data in the previous

Stanford University study. While MRTA measurements of EI were unbiased (mean difference = 0.2 ± 0.8%, p=0.67) with respect to QMT, MRTA measurements of EI in the Stanford University study were strongly biased (mean difference 53%± 9.3 %, $p<10^{-4}$) (29). Moreover, in this study, paired MRTA and QMT measurements of EI in individual ulnas were interchangeable within limits of agreement ±5%, whereas the Stanford study was only able to demonstrate limits of agreement in excess of ±40%. In the present study, great pains were taken to match MRTA and QMT testing conditions, whereas there were substantial differences between MRTA and QMT test conditions in the Stanford study (29). Whether the improved performance demonstrated in this study is attributable to improved experimental controls or to improved technology is unknown.

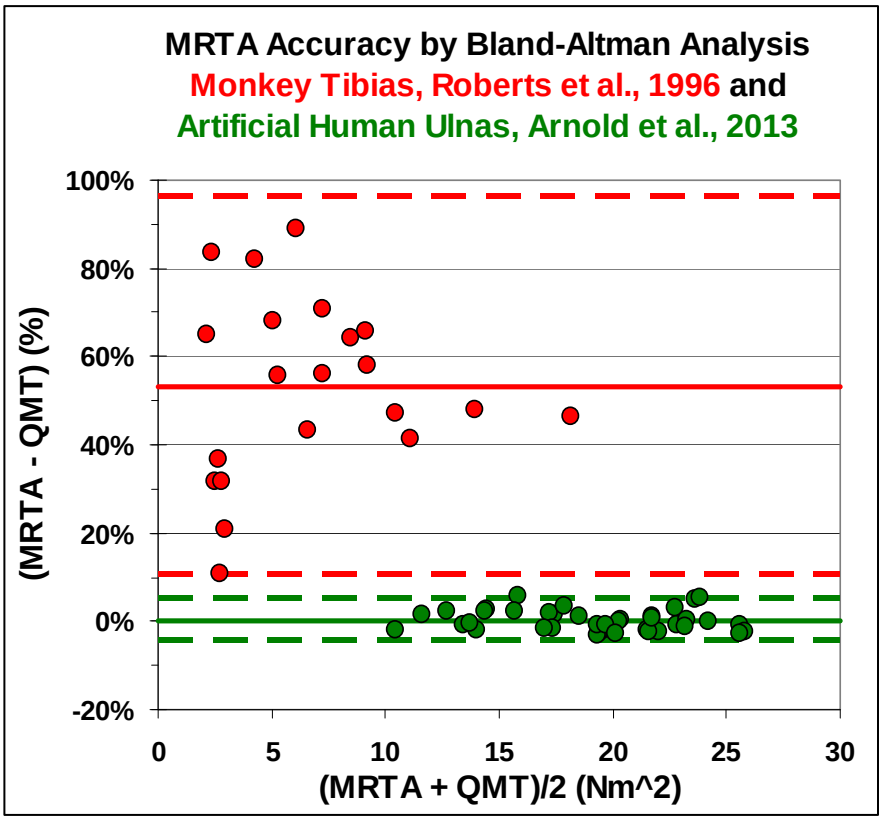

Fig. 85
Bland-Altman analyses of paired QMT and MRTA EI. The red data are from the previous Stanford University study and the green data are from the present study. The solid lines represent the mean of measurements and the dotted lines are the limits of agreement, i.e., 95% confidence intervals, of individual measurements.

Clinical Application of Findings

Within this study, MRTA measurements of EI in artificial human ulnas would be sufficiently precise, repeatable, and accurate for clinical applications.

The repeatability of a measurement determines the magnitude of the minimum treatment effect that can be detected in an individual (approximately two times the repeatability), and the number of participants that must be studied in a clinical trial in order to detect a smaller treatment effect. For example, a previous study of the effects

of resistance exercise on ulna EI and BMD had to accumulate data from 32 participants for twenty weeks in order for the treatment effect on BMD to become sufficiently large (2.7%) for it to be distinguished from the 1.1% repeatability of DXA (22). Several additional participants also had to be studied in order to overcome the 28% subject attrition rate during such a long experimental protocol (22). By contrast, only 22 participants were needed to detect a 32% increase in ulna EI against the unreported repeatability of MRTA measurements. In the research described in this thesis, the 3.1% repeatability of MRTA measurements of EI suggests that effects of resistance exercise on ulna EI could be detected with even fewer participants, and in shorter periods of time, which would greatly reduce the cost of such studies.

The ±5% limits of agreement between MRTA and QMT measurements of EI were, substantially smaller than the assumed clinically important difference of 10%. A 5% error in an EI measurement of 20 Nm^2 would lead to measurements between 19 and 21Nm^2, which would not affect clinical decisions. Even the ±4% to ±6% uncertainty in the limits of agreement in this study would be, substantially less than the assumed 10% clinically important difference.

Measurements of bone properties are clinically useful only insofar as they accurately estimate fracture risk. Despite the strong association found in this study between MRTA measurements of EI and bending strength, the clinical utility of MRTA-measured ulna EI in estimating fracture risk still remains uncertain. A large epidemiological study would need to be performed to identify some threshold of ulna EI that discriminated better than BMD measured by DXA between those who do and

do not subsequently fracture. The greatest likelihood of success in this effort would probably be the diagnosis of senile osteoporosis, because 80% of fractures in men and women over the age of 60 occur in cortical bone (15, 27).

Significance

The validation of Ohio University's MRTA system will be of interest to investigators inside and outside of the Ohio University community. Having determined the accuracy, precision, and repeatability of MRTA in measuring EI and predicting bone strength in artificial human ulnas, the MRTA lab at Ohio University plans to conduct similar experiments on human cadaveric ulnas. If this research finds similar results, then the MRTA lab expects to use the device in a series observational and experimental research studies to explore its clinical utility. One observational study is expected to compare ulna EI in clinically contrasting groups, such as the dominant and non-dominant arms of athletes participating in sports that mechanically load the body symmetrically (e.g., swimming) and asymmetrically (e.g., baseball). Clinical trials are expected to investigate effects of mechanical loading (i.e., resistance and plyometric exercise) and unloading (i.e., casting) on ulna EI.

If such studies confirm the clinical utility of MRTA technology, investigators outside of Ohio University can be expected to use MRTA systems to investigate a broader range of clinical applications of the technology such as senile osteoporosis. The MRTA lab at OU plans to facilitate such research by constructing several MRTA devices for use by collaborators at other institutions. Successful demonstration of the

utility of MRTA technology could result in it becoming the first clinically applicable device for making non-invasive, direct, and radiation free measurements of cortical bone *in vivo* for determining fracture risk, monitoring bone growth in children, and diagnosing osteoporosis.

REFERENCES

1.Arnold PA, Horne NKV, Bowman L, et al., editors. New wrist support improves mechanical response tissue analysis (MRTA) of ulna bone strength measurements. Ohio University Student Research and Creative Activity Expo; 2012 May 2012; Athens, OH.

2. Borders S, Petersen KR, Orne D. Prediction of bending strength of long bones from measurements of bending stiffness and bone mineral content. J Biomech Eng 99:(40-4), 1977.

3. Cotton J, Bowman L, Stroud C, editors. Ulna simulation assesses sensitivity to bone elastic modulus variations in a MRTA test. American Society of Biomechanics Annual Meeting; 2012 August 15-18, 2012; Gainesville, FL.

4. Crenshaw TD, Peo J, E. R., Lewis AJ, et al. Bone strength as a trait for assesing mineralization in swine: a critical review of techniques involved. J Anim Sci 53:(827-35), 1981.

5. Cristofolini L, Viceconti M. Mechanical validation of whole bone composite tibia models. J Biomech 33:(279-88), 2000.

6. Cristofolini L, Viceconti M, Cappello A, et al. Mechanical validation of whole bone composite femur models. J Biomech 29:(525-35), 1996.

7. Dunlap JT, Chong AC, Lucas GL, et al. Structural properties of a novel design of composite analogue humeri models. Ann Biomed Eng 36:(1922-6), 2008.

8. Office of the Surgeon General. Bone health and osteoporosis: a report of the surgeon general. 2004.

9. Office of the Surgeon General. The surgeon general's report on bone health and osteoporosis: what it means to you. 2012.

10. Grover P, Albert C, Wang M, et al. Mechanical characterization of fourth generation composite humerus. Proc Inst Mech Eng H 225:(1169-76), 2011.

11. Haggerty JJ. A Boon for Bone Research. NASA Spinoff:(48-9), 1996.

12. Heiner AD. Structural properties of fourth-generation composite femurs and tibias. J Biomech 41:(3282-4), 2008.

13. Jarvinen TL, Sievanen H, Kannus P, et al. Dual-energy X-ray absorptiometry in predicting mechanical characteristics of rat femur. Bone 22:(551-8), 1998.

14. Jurist JM, Foltz AS. Human ulnar bending stiffness, mineral content, geometry and strength. J Biomech 10:(455-9), 1977.

15. Kanis JA, Johnell O, Oden A, et al. Ten year probabilities of osteoporotic fractures according to BMD and diagnostic thresholds. Osteoporos Int 12:(989-95), 2001.

16. Kiebzak GM, Box JH, Box P. Decreased ulnar bending stiffness in osteoporotic Caucasian women. J Clin Densitom 2:(143-52), 1999.

17. Lau RY, Guo X. A review on current osteoporosis research: with special focus on disuse bone loss. J Osteoporos 2011:(293808), 2011.

18. Leppanen O, Sievanen H, Jokihaara J, et al. Three-point bending of rat femur in the mediolateral direction: introduction and validation of a novel biomechanical testing protocol. J Bone and Miner Res 21:(1231-7), 2006.

19. Marks SC. Structure and Development of the Skeleton. Second ed: Academic Press; 2002. p. 3-15.

20. McCabe F, Zhou LJ, Steele CR, et al. Noninvasive assessment of ulnar bending stiffness in women. J Bone Miner Res 6:(53-9), 1991.

21. Miller LE, Nickols-Richardson SM, Wootten DF, et al. Isokinetic resistance training increases tibial bending stiffness in young women. Calcif Tissue Int 84:(446-52), 2009.

22. Miller LE, Wootten DF, Nickols-Richardson SM, et al. Isokinetic training increases ulnar bending stiffness and bone mineral in young women. Bone 41:(685-9), 2007.

23. Myburgh KH, Charette S, Zhou L, et al. Influence of recreational activity and muscle strength on ulnar bending stiffness in men. Med Sci Sports Exerc 25:(592-6), 1993.

24. Myburgh KH, Zhou LJ, Steele CR, et al. In vivo assessment of forearm bone mass and ulnar bending stiffness in healthy men. J Bone Miner Res 7:(1345-50), 1992.

25. NIH Consensus Development Panel. Osteoporosis prevention, diagnosis, and therapy. Jama 285:(785-95), 2001.

26. Papini M, Zdero R, Schemitsch EH, et al. The biomechanics of human femurs in axial and torsional loading: comparison of finite element analysis, human cadaveric femurs, and synthetic femurs. J Biomech Eng 129:(12-9), 2007.

27. Riggs BL, Wahner HW, Dunn WL, et al. Differential changes in bone mineral density of the appendicular and axial skeleton with aging: relationship to spinal osteoporosis. J Clin Invest 67:(328-35), 1981.

28. Rittweger J, Simunic B, Bilancio G, et al. Bone loss in the lower leg during 35 days of bed rest is predominantly from the cortical compartment. Bone 44:(612-8), 2009.

29. Roberts SG, Hutchinson TM, Arnaud SB, et al. Noninvasive determination of bone mechanical properties using vibration response: a refined model and validation in vivo. J Biomech 29:(91-8), 1996.

30. Seeman E, Delmas PD. Bone quality--the material and structural basis of bone strength and fragility. N Engl J Med 354:(2250-61), 2006.

31. Siris ES, Miller PD, Barrett-Connor E, et al. Identification and fracture outcomes of undiagnosed low bone mineral density in postmenopausal women: results from the National Osteoporosis Risk Assessment. Jama 286:(2815-22), 2001.

32. Steele CR, Zhou LJ, Guido D, et al. Noninvasive determination of ulnar stiffness from mechanical response--in vivo comparison of stiffness and bone mineral content in humans. J Biomech Eng 110:(87-96), 1988.

33. Turner CH, Burr DB. Basic biomechanical measurements of bone: a tutorial. Bone 14:(595-608), 1993.

34. Vernikos J, Schneider VS. Space, gravity and the physiology of aging: parallel or convergent disciplines? A mini-review. Gerontology 56:(157-66), 2010.

35. Wynnyckyj C, Omelon S, Savage K, et al. A new tool to assess the mechanical properties of bone due to collagen degradation. Bone 44:(840-8), 2009.

36. Yeni YN, Brown CU, Wang Z, et al. The influence of bone morphology on fracture toughness of the human femur and tibia. Bone 21:(453-9), 1997.

37. Zebaze RM, Ghasem-Zadeh A, Bohte A, et al. Intracortical remodelling and porosity in the distal radius and post-mortem femurs of women: a cross-sectional study. Lancet 375:(1729-36), 2010.